DEVELOPMENT OF ARRAYED STRUCTURES USING REVERSE EDM (R-EDM)

Thesis Submitted In Partial Fulfilment

of the Requirements for the Award of

Master of Technology

In

Production Engineering

By

KONA NAGEENDRABABU

Department of Mechanical Engineering

National Institute of Technology

Rourkela (India)

2015

Development of Arrayed Structures
Using Reverse EDM (R-EDM)

Thesis Submitted in Partial Fulfilment

of the Requirements for the Award of

Master of Technology

In

Production Engineering

By

KONA NAGEENDRABABU

ROLL.NO. 213ME2413

Under The Guidance of

Dr. S. GANGOPADHYAY

Department of Mechanical Engineering

National Institute of Technology

Rourkela (India)

National Institute of Technology

Rourkela (India)

CERTIFICATE

This is to certify that the thesis entitled ― **Development of Arrayed Structures Using Reverse Edm (R-Edm)** submitted to the National Institute of Technology, Rourkela by **KONA NAGEENDRABABU**, bearing Roll no. **213ME2413** for the award of the Degree of Master of Technology in Mechanical Engineering with specialization in―**Production Engineering** is a record of bonafide research work carried out by him under my supervision and guidance. The results existing in this thesis has not been, to the best of my knowledge, submitted to any other University or Institute for the award of any degree or diploma. The thesis, in my opinion, has reached the standards fulfilling the requirement for the award of the degree of Master of technology in accordance with regulations of the Institute.

Date

Dr. S. Gangopadhyay

Assistant Professor

Department of Mechanical Engineering

National institute of Technology, Rourkela

ACKNOWLEDGEMENT

I wish to express my sincere gratitude to my supervisor Dr. S. Gangopadhyay, for giving me an opportunity to work on this project, for his guidance, encouragement and support throughout this work and my studies here at NIT Rourkela. His impressive knowledge, technical skills and human qualities have been a source of inspiration and a model for me to follow.

I express my sincere gratefulness to Dr. S. S. Mahapatra, Head of the Department, Mechanical Engineering, and NIT Rourkela for giving me an opportunity to work on this project and allowing me the access to valuable facilities in the department.

I am also thankful to Mr. Talla Gangadharudu Ph.D. research scholar and my friends for their consistent support, immense help and continuous encouragement for the completion of this project work. It's my wish to express my gratitude towards my loving parents and family for their eternal effort.

Date   KONA NAGEENDRABABU

                                                      Roll. NO. 213ME2413

ABSTRACT

In recent years, reverse electric discharge machining (R-EDM) has been developed as a method for the fabrication of arrayed structures which find applications in the fabrication of fins and component assembly. In this study, the feasibility of R-EDM process in the fabrication of arrayed features of $\emptyset$ 3 mm and height 2 mm on mild steel has been studied through response surface methodology (RSM) based experimentation. The influence of machining parameters i.e., peak current (I_p), pulse-on time (T_{on}) and flushing pressure (F_p) on some of the vital response characteristics like material removal rate (MRR), surface roughness (SR), taper, cylindricity error and micro hardness and surface morphology of the pillared structures has been investigated. Further, a hybrid optimization method i.e., principal component analysis (PCA) based grey relational analysis (GRA) technique, is utilized to obtain optimal parameter combination with an aim to improve machining conditions for fabrication of arrayed features during R-EDM process. Analysis of variance (ANOVA) results shows that I_p has significant effect followed by T_{on} on MRR and I_p has major contribution towards SR, taper and cylindricity error. Micro hardness has maximum value in heat affected zone (HAZ). The optimal parameter combination based on PCA based GRA is found to be I_p = 10 A, T_{on} = 100 µs and F_p = 0.3 kg/cm^2 which was further ascertained using confirmatory test.

Keywords: Arrayed features, cylindricity error, micro hardness, optimization, taper angle, surface morphology.

CONTENTS

LIST OF FIGURES

LIST OF TABLES

CHAPTER 1

INTRODUCTION

1. Concept of Surface Texturing

Surface texturing is generally defined as modification of surface of a substrate or work piece material by means of imparting suitable surface roughness or fabricating required surface structures. Hence textured surfaces in other way called as structured engineered surfaces. The term surface texturing was coined in early 1930s but it was used in 1940s for the first time when honing method was applied to produce stripes on cylinder-liner surface in order to improve frictional characteristics [1]. From there onwards, the technology of texturing has spread widely in the fields of industrial, biomedical and military applications.

1.1 Methods for fabricating textured surfaces

Depending on surface requirement and texture method used, texturing can be formed as micro pits or micro pillars. The word textured surfaces used only to describe surfaces containing engineered structures (micro holes, micro rods). In general, fabrication processes can be categorized based on the way material is modified in order to generate surface texture, are briefly discussed below [2]

- Material adding methods

- Material removal methods

- Material displacement technologies

- Self- forming method

Table 1. Types of surface texturing methods

Mechanism	Description	Methods
Addition of material	Chemical or physical processes are employed to form textured surfaces at micro or nano level	Chemical based: chemical vapour deposition (CVD),Electro deposition (electroplating) Physical based: Ink jet printing, physical vapour deposition (PVD) Thermal implantation: Laser micro cladding
Removal of material	Surface texture formation by removal of substrate material to develop micro holes or micro pillars	High temperature based: laser beam texturing (LBT),Electrical discharge texturing (EDT), micro EDM, Electron beam texturing (EBT) Etching: chemical etching (ECT) Mechanical removal: CNC ultrasonic machining, patterned erosion process
Displacement of material	Developing textures by plastic deformation and replacing material from one location to another	Mechanical induced: Embossing technique, laser shock peening Chemical induced: molecular migration, surface wrinkling
Self -forming	This technique takes longer time for fabrication of textures i.e., initially formation of wear resistant regions then texture results from gradual surface wear	Texture auto formation: Thermal implantation of hard phases Self-adaptive functional surfaces

The current study focusses on some of material adding methods and material removal methods and the same are discussed briefly in the following sections.

1.1.1 Material adding methods

In this method texturing on substrate is done by deposition of special ink which promotes chemical reactions and develops a patterned surface. In case of metallic substances, in order to avoid electrical discharges between substrate and deposited material the surface is coated with a thin layer of coating during texturing process [3].One of the chemical based processes is chemical vapour deposition process (CVD) in which the pattern development takes place due to use of mask generally contains adhesion inhibitors deposited on the substrate by micro contact printing method or stamping [4].The advantage of CVD method is felicity in texturing any geometry such as micro pillars or micro holes with heights varying from nano meter (nm) to few (μm).This method is equally applicable for both planar and cylindrical surfaces. This process finds its applications in areas such as manufacturing, optics, and electronics etc. [5].

Another chemical based method is physical deposition method. The inkjet printing process one of the physical deposition methods used to form micro or nano semi spheres (single drop deposition) or micro pillars (successive drop deposition) as shown in Fig. 1.1. [6].
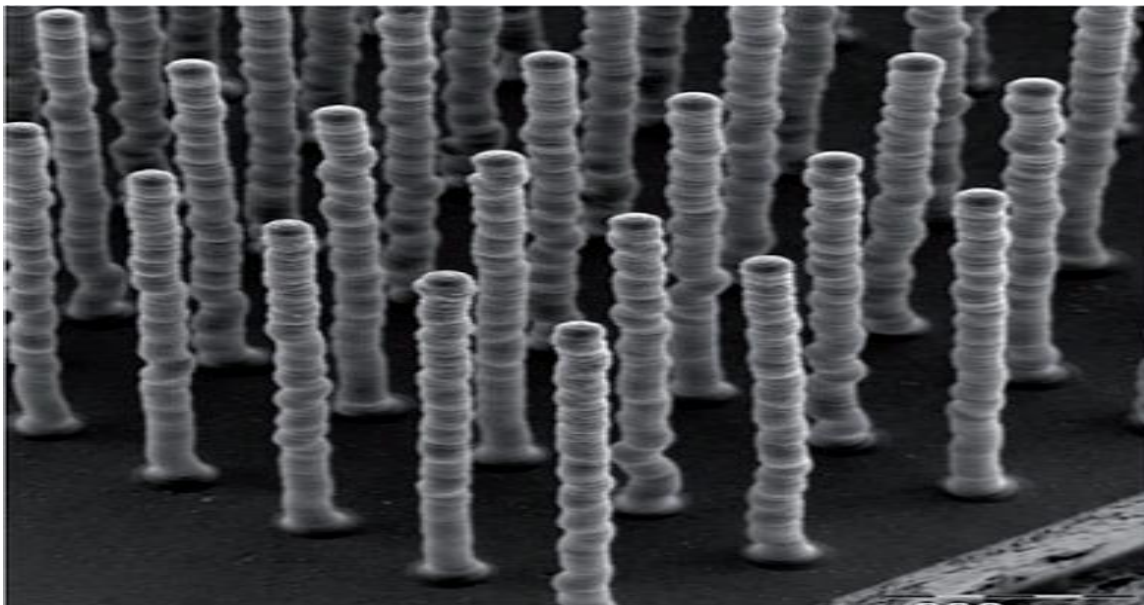
Fig.1.1. Deposition of micro pillars on TiO_2 by inkjet printing [6]

Because of point by point method of deposition ink jet printing develops structures with good accuracy ranging from 5 and 900 µm and lateral dimensions of 20 and 200 µm [7]. Variety of pattern geometry can be developed through PVD and involves less processing temperature compared to high temperature methods such as laser, focused ion beam etc.

1.1.2 Material removal methods

Removing material technologies utilizes high temperatures for texturing process (laser technologies, electrical discharge methods, electron beam or ion beam methods), chemical reactions (etching) or a mechanical process (grinding, honing, ultrasonic machining and blasting). Though the substrate is subjected to high temperatures these techniques are capable of forming variety of continues or discontinues textures.

Laser texturing

Laser texturing is done by the principle based on ablation process i.e. heating and vaporisation of substrate. Semi spherical textures in the form of dimples are known shapes usually developed by laser texturing method. Texture accuracy depends on focussing of laser beam to substrate surface while depth and aspect ratio are maintained by proper pulse duration, wave length and power. Texture dimensions and complexity of geometry are directly related to higher power and longer wavelengths [8]. Laser texturing involves surface defects such as bulges or burrs and another important aspect is thermal effect of laser beam that significantly changes the metallurgical properties of substrate.

Electro chemical machining (ECM)

Electro chemical machining (ECM) is another method that can be utilized to texture complex geometries including inner and outer cylindrical surfaces on any hard and soft materials. The main advantage of this method is that it does not involve any mechanical or thermal stresses [9].

Electric discharge machining (EDM)

Electrical discharge machining (EDM) is a non-traditional machining method in which the material removal takes place due to electrical spark generated between the tool and the work piece. This method uses thermo electric source of energy for machining extremely low machinability materials, difficult to cut and high strength alloys and all electrically conductive materials. The basic scheme of EDM is illustrated in Fig.1.2.
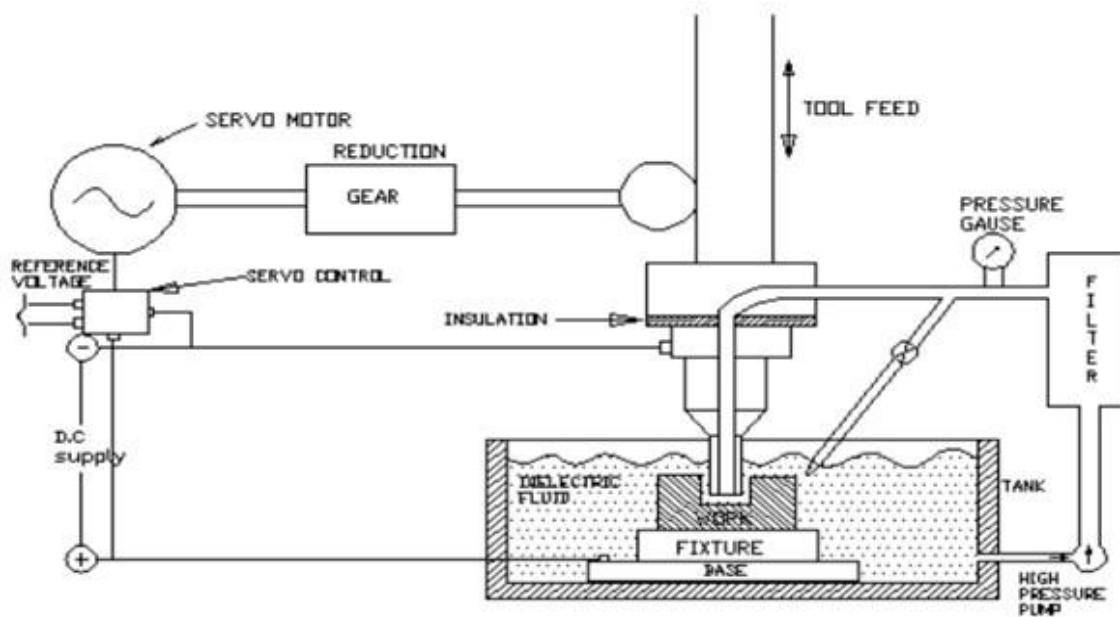
Fig.1.2 Experimental setup of electric discharge machining [10]

Principle of EDM

The material removal mechanism involves conversion of electrical energy into thermal energy there by producing electrical discharges between the tool (cathode) and work piece (anode) which are submerged in dielectric liquid medium. The cathode and anode are connected to DC supply. Kerosene, deionized water and EDM oil are the commonly used dielectric fluids. The electrodes are separated by a very thin gap known as spark gap of about 0.025 mm. The gap is controlled by servo mechanism. When electrodes are supplied with sufficient gap voltage the dielectric breakdown takes place and develops high thermal energy.

The thermal energy so produced generates a plasma channel between tool and work piece. When the current supply is turned off, break down of plasma channel occurs and causes sudden decrease in temperature. The breakdown of plasma channel results in acceleration of electrons from cathode to anode as shown in Fig. 1.3. Electrons from cathode move at a faster rate and collide with molecules of dielectric fluid and create more positive ions and electrons. Now the bunch of electrons moves towards anode whereas the positive ions accelerated towards cathode. The impact of these positive ions and electrons to the cathode and anodes generates heat energy.
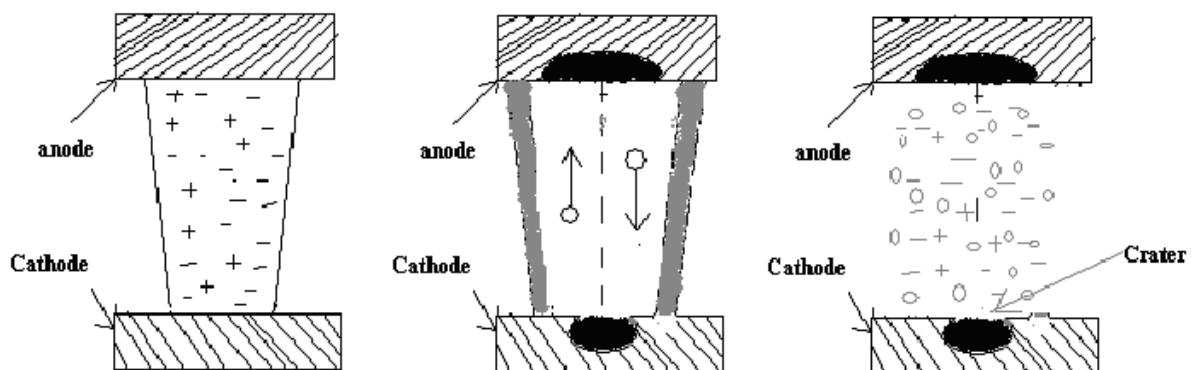
Fig.1.3 Formation of plasma channel during EDM [11]

In such a way electrical discharge occurs at a point where cathode and anode are melted and vaporized thus lead to the formation of crater on both tool electrode and work piece. The molten material in form of debris will be flushed away from the electrode gap by the flow of dielectric fluid. At the end of each discharge, electrons and positive ions will recombine due to temperature drop of plasma channel. In order to maintain stability in EDM process, the pulse interval between the next discharges should not be so long and not too short. If the pulse interval is long the plasma channel produced can be fully de-ionized and the dielectric breakdown strength around the previous discharge can be recovered by the time next voltage

charge is supplied and short pulse duration results in poor surface finish and instability in the process [11].

1.1.3 Important parameters of EDM

(a) Pulse-on time (T_{on}): It is the time period during which the current is passed through the tool within a short gap called as spark gap. It directly influences the amount of material removal from the work piece. Pulse-on time is also called pulse duration measured in micro seconds (µs). Material removal rate cannot be increased alone by increasing T_{on} but proper selection of peak current (I_p) is also required for the efficient removal of material from the work piece. At constant current and duty factor, MRR found to be decreased with higher T_{on}. This causes rapid expansion of plasma channel results in less energy density on the anode.

(b) Pulse of time (T_{off}): It is the time period during which no machining takes places i.e., idle time period. During this period dielectric fluid is allowed to remove the molten material from the work piece surface.
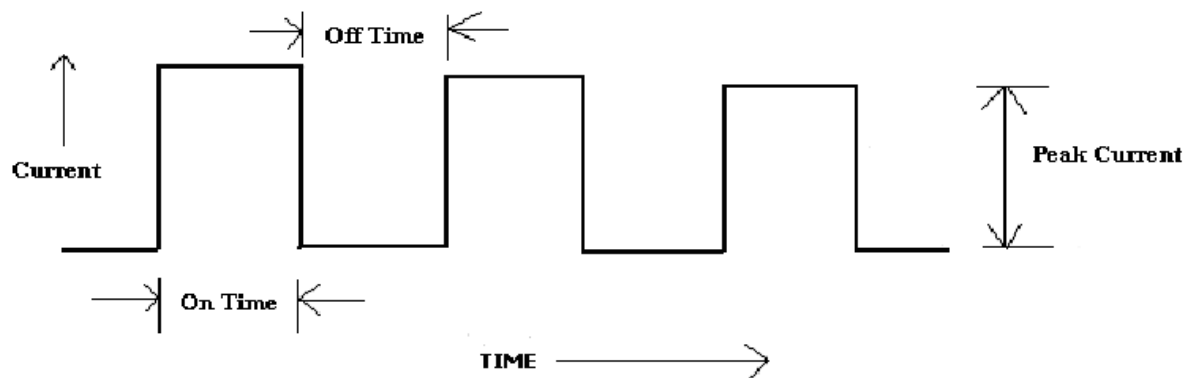
Fig.1.4 Pulse wave form [12]

(c) Electrode gap: It is the gap maintained between the tool and the work piece during the EDM process. It can be maintained by servo control mechanism.

(d) Duty cycle (τ): It is the percentage of pulse-on time to total cycle time (pulse-on time plus pulse off time). It defines the degree of machining efficiency.

$$\text{Duty cycle} = \frac{T_{on}}{T_{on} + T_{off}}$$

(e) Polarity: It indicates the polarity of tool or work piece to which they are connected i.e., positive or negative. It found that material removal is more when tool is connected to positive polarity and work piece is connected to negative terminal.

1.1.4 Dielectric fluid

The dielectric fluid has the following functions

(a) It acts as an insulator between electrode and work piece.

(b) It acts as a coolant to draw away the heat generated due to sparks.

(c) It maintains a constant resistance across the electrode gap.

(d) It carries away eroded metal particles with it.

The dielectric fluid chosen should be non-toxic and chemically inert with respect to tool material and work piece material. The properties of dielectric fluid should be such as to cause deionisation of the medium very quickly after discharging and make it effective insulating medium during the next charging operation. The viscosity should be low so that it flushes away the eroded particles as soon as produced. Various fluids which are used as dielectric fluids are transformer oil, kerosene, mineral oil, and hydrocarbon or paraffin oils.

1.1.5 Tool material

The primary requirements of any tool material are

1. It should be electrically conductive.

2. It should have good machinability.

3. It should have low erosion rates.

4. It should have high melting point.

5. It should have high electron emission.

The commonly used electrode materials are copper, brass, copper tungsten alloy, silver tungsten alloy, tungsten carbide, graphite and copper graphite.

1.1.6 Applications of EDM

1. EDM is widely used for machining burr free intricate shapes, narrow slots and blind cavities.

2. Almost any geometry i.e., negative of the tool can be generated on a work piece if suitable tool can be fabricated.

3. It can drill small holes of about 0.13 mm in diameter with virtually no bending and drifting of hole.

4. EDM is particularly useful for machining of small holes, orifices or slots in diesel fuel injection nozzles, or in aircraft engines, air brake valves and so on.

5. Internal threads and internal helical gears can be cut with great accuracy.

1.1.7 Advantages of EDM

1. EDM can be used for machining any material that is electrically conductive, thus including metals, alloys and most carbides.

2. The melting point, hardness, toughness or brittleness of the material poses no problems. Due to this EDM can be used for machining materials that are too hard or brittle to be machined by conventional methods.

3. The method does not leave any burrs or chips on the work piece.

4. Cutting forces are virtually zero, so very delicate and fine work can be done.

5. The process dimension repeatability and surface finish obtained in finishing are extremely good.

1.1.8 Limitations of EDM

1. Only electrically conductive machines can be machined. Thus, non-metallic materials such as plastics, glass cannot be machined.

2. Electrode wear and over cut are serious problems.

3. Material removal rate is low, therefore this process should only be used where other conventional machining processes are not suitable as machining costs are high.

4. Surface cracking may takes place in some materials owing to their affinity to become brittle at room temperature especially when energy per pulse is used.

1.1.9 Variants of EDM

Die sinking EDM

Die sinking EDM is the most common type of EDM process in which shape of the machined profile is the replica of tool electrode. This method can be used for the production of complex cavities with high accuracy. A number of EDM methods have been developed based on this die sinking EDM configuration for the machining of difficult to cut materials or super alloys used in the space and aeronautical applications. Wire- cut EDM (WEDM), micro EDM (EDM) are some of the most popular EDM variants based on their capability to machine intricate shapes and geometries on highly conductive, high strength and temperature resistant materials.

Electric discharge texturing (EDT)

Electric discharge texturing (EDT) works on the same principal of EDM that can be used for developing textures on any electrically conductive materials such as hardened steel, tungsten carbide and nonconductive materials like ceramics [13]. EDT is usually used for roll mill texturing in which the roll is treated as one electrode, separated by dielectric fluid such as hydrocarbon or paraffin oil, from a tool electrode. Due to discharge between the electrodes minute craters will form on the roll [14]. EDT can also be used to develop textures on rake face of the tool in order to enhance lubrication and reduce the machining forces, which improves the tool life [15].Since EDT is a high temperature process there is a possibility of change in microstructure of roll surface. The surface damage can be minimized by controlling the process parameters of EDT process.

Advantages of EDT

1. Intrinsic shapes with sharp corners and angles can be accurately developed.

2. Textures with dimensions smaller 100μm can be produced.

3. High precision along with low surface roughness can be obtained.

4. Because of absence of tool rotation the process does not involve mechanical stresses.

Limitations

1. Limited size of work piece due to low material removal rates (100 mm^3/min).

2. Formation of heat affected zone and recast layer.

Reverse micro – EDM (R-MEDM)

Electro discharge machining process can be used not only for machining holes or cavities in work piece, but also for fabricating arrayed structures of different cross-sections by feeding or scanning an electrode (cathode) having an array of cavities machined by CNC drilling or CNC milling or any other hole machining process. After applying a positive voltage to work piece material (anode), the tool (electrode) with array of cavities fed down in such a way that due to electric sparks between the tool and the work piece selective material removal will take place on anode in such a way that shape of the tool is reproduced. Hence the cross section of anode is a reverse replica of a cross section of hole array on the tool i.e. the regions on surface of work piece which correspond to cavities are not machined and remain resulting in a projection at each cavity. The size and accuracy of cavities on work piece largely influenced by setting of tool in the machine spindle and the motion of electrode can be controlled by controlling the displacement along Z-axis. This process is usually called reverse micro EDM (R-MEDM) [16].
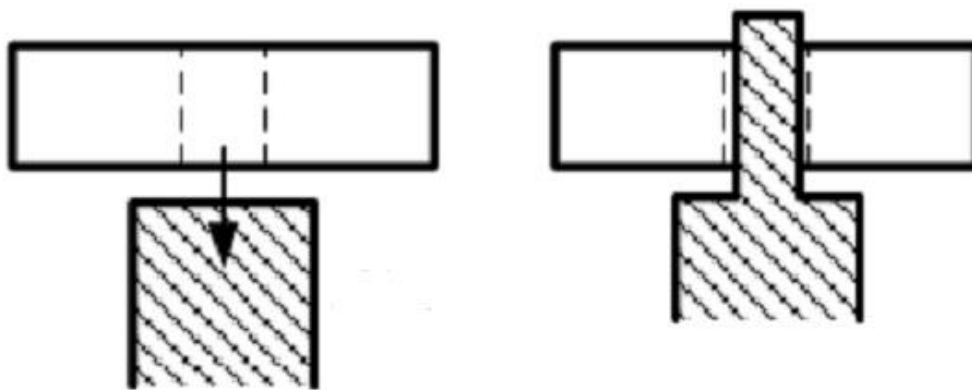
(a) Work piece before R-MEDM   (b) Work piece after R-MEDM

Fig. 1.5 Basic principle for Fabrication of arrayed features using R-MEDM [16]

Hence, reverse electrical discharge machining, a variant of conventional EDM, the mechanism of material removal is same, the key difference being, extruded arrayed features are fabricated in the reverse EDM while a cavity is machined from cylindrical tool in EDM as shown in Fig. 1.6. The process mechanics and response of EDM and R-MEDM primarily differ due to variation in electrode geometries. In reverse EDM, since rather a large surface area of work piece is under machining debris and other dirt particles are accumulated in the gap between the cavities of tool and arrayed structures preventing stable discharge. For stable machining, dielectric fluid must be flushed and the debris must be removed from the machining area, often accomplished through rotation of tool electrode. In R-MEDM, however for fabricating arrayed structures of different cross sections, it is impossible to rotate the tool electrode usually, in die sinking EDM where a tool electrode is not rotated, the molten materials are not easily removed and even stick to the electrode and the work piece, causing short current and welding. Goto et al. found that 'short bridge' occurs because of molten material. In EDM, when short current is perceived, the tool electrode goes a few μm back till short current vanishes. Therefore, in R-MEDM, in which the tool electrode does not rotate, unstable machining occurs [17].

(a)   (b)
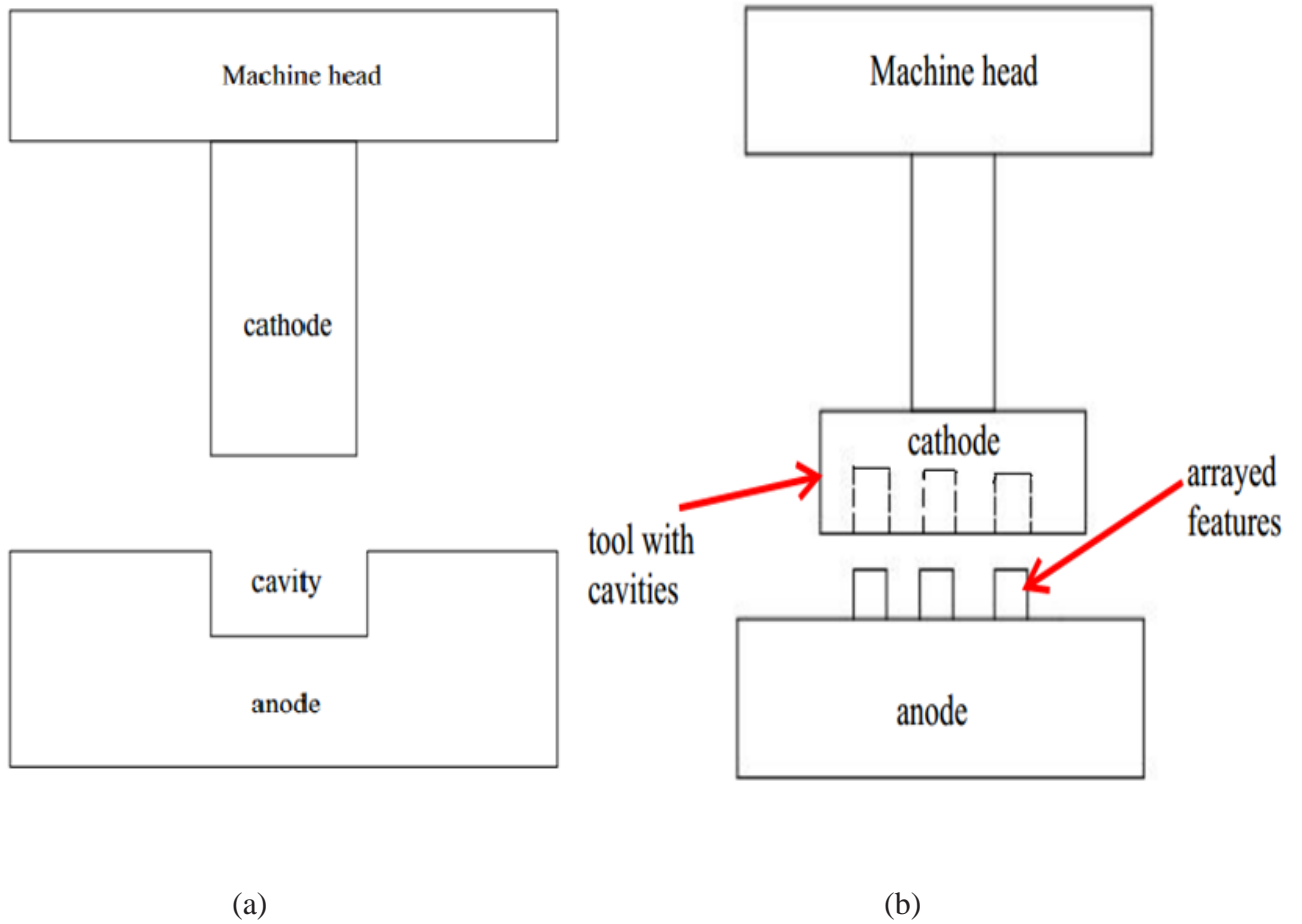
Fig.1.6 Difference in geometries of machined surfaces (a). EDM (b). R-MEDM

Chapter 2

Literature review

2.1 Fabrication of Textured surfaces

Chamaran et al. found that the micro EDM (MEDM) process was capable for fabricating high aspect ratio arrayed features of diameter 5µm required in various micro engineering applications such as fuel injectors, fins in automobile radiators, biomedical sensor devices [18].

Joshi et al. fabricated high aspect ratio arrayed micro-structures and textured surfaces (Fig. 2.1) used in applications such as electrical contacts, printing heads, electrodes for micro-batteries, injection nozzles, nano-material delivery systems, biomedical implants with reverse micro-electrical discharge machining (R-MEDM) process. The mechanism of M-REDM process was compared with the other micromachining processes presently available for the fabrication of arrayed micro-features and found that R-MEDM offers better performance in the development of arrayed features compared to micro-milling, micro-wire EDM, micro-wire electrical discharge grinding (EDG) [19].
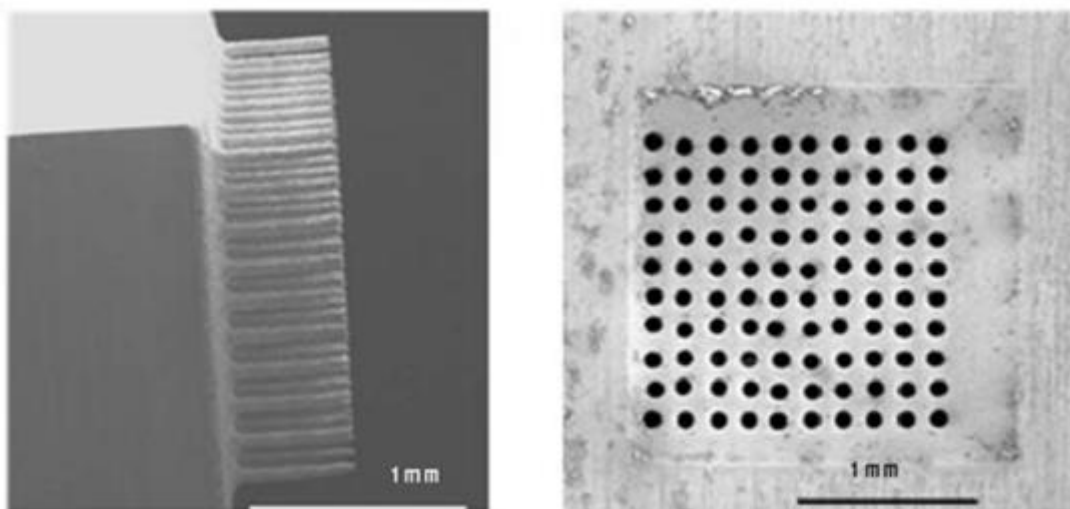
Fig. 2.1 Fabrication of Arrayed structures using R-MEDM [19]

Wang et al. suggested that reversible micro electric discharge machining can selective deposit and remove material on work piece surface by pulse discharge between anode and cathode using ordinary EDM machine tool. Experimentations showed electrode materials such as steel, copper and tungsten, can be deposited on steel work-piece surface to form micro cylinder of diameter 100-240 μm and height of 1000-2500 μm and the results showed that the micro cylinders formed by electric discharge deposition were compact, hard and combined with work piece surface closely [20].

Kim et al. fabricated micro electrodes of various shapes by reverse electrical discharge machining and these multiple-tipped micro electrodes were then utilized to machine micro hole arrays, grooves on stainless steel using micro electrochemical machining [21].

Yi et al. positively fabricated 3×3 and 4×4 arrays on Cu using 100μm thick AISI 303 stainless steel plates, which in turn used for machining 6×6 and 16×16 cavity patterns on metal plates for applications in organic thin film transistors (OTFTs) [22]. By providing ultrasonic vibrations at 20 kHz and 1μm amplitude to the plate electrode during reverse EDM process it was found the processing duration for fabricating arrayed features was reduced by 2.5 times and also surface finish was improved significantly [23].

Hwang et al. fabricated an array of 40×40 (1600 pins of ϕ30μm, length 625μm) on WC over 6.8×6.8mm^2 area with high hardness, high density and uniformity in diameter. Vibration assisted peck drilling was employed to drill the 40×40 hole array on 0.6mm brass plate[24]. Textured surface containing micro pillars of 40–50 μm in diameter spaced at 35 μm have been created on Ti6Al4V rods via vibration assisted reverse micro electrical discharge machining process [25].

Jin et al. deposited micro cylinders on brass, steel and tungsten by exchanging the polarities of electrode and work piece during the normal EDM process as shown in Fig 2.2. The outcomes showed that with proper selection of processing parameters the deposition machining was stable and consistent and also found that the deposited material was dense in centre, while it was looser and ring-shaped at the edges because the liquefied metal spreads from centre to edges under the gravity, which creates the parabolic profile and found that the hardness of the deposited material is higher than the parent material due to high cooling rate [26].

(a) Brass micro cylinder   (b) End surface   (c) Steel micro cylinder   (d) Tungsten micro cylinder
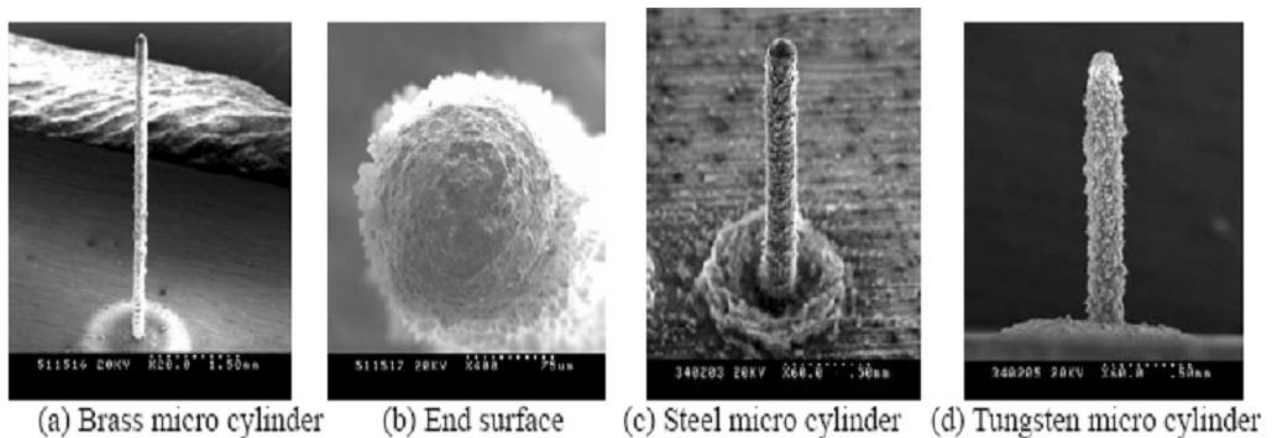
Fig. 2.2 Micro cylinders formed by EDM deposition [26]

Fofonoff et al. used wire-EDM for developing micro electrode array assemblies used in biomedical devices. Microelectrode arrays were fabricated using a zinc coated brass 100 µm wire from titanium- aluminium-vanadium alloy (Ti90-Al6-v4), stainless steel and tungsten carbide. The cut consists of three phases with pulse duration of 0.2µs, machining voltage of -80V, -80V and 120V with respect to work piece and machining frequencies of 200 kHz, 1 MHz and 1 MHz respectively. It was found that wire electro discharge machining process could be suitable for machining features with high aspect ratio [27].

Takahata et al. used LIGA (lithographic) process for fabricating array of 400 Cu electrodes of 20 μm diameter and examined the scaling issues on arrayed features and constraints in the fabrication and usage of high aspect ratio LIGA-fabricated electrode arrays and the restrictions enacted by the pulse discharge circuits on machining rates [28].

Gupta et al. focused on micro electrical discharge machining process of pyrolytic carbon (PyC) to produce pillar type structure as depicted in Fig. 2.3 which are utilized in various biomedical devices like cardiovascular implants and finger prosthesis [29].
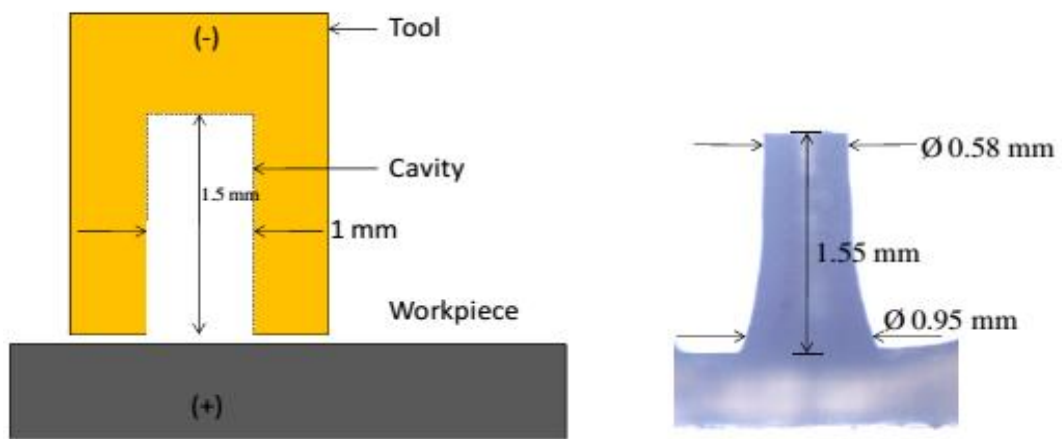
Fig. 2.3 Pillared structure machined using reverse micro EDM [30]

Sachin et al. compared the process mechanics of micro-electrical discharge machining (MEDM) and reverse-micro-electrical discharge machining (R-MEDM). Studies shown that R-MEDM is more stable than MEDM as per V-I signal characteristics and can therefore be operated at higher values of capacitance and voltage [30]. Further it was observed that R-MEDM effects in higher material erosion rates but has a higher surface roughness value compared to that produced by MEDM due to debris entrapment and subsequent welding to the machined features.

Weiliang et al. successfully developed microelectrode array and micro hole array by combined micro WEDM and EMM (Electrochemical micro machining). Micro electrode array of 10×10 having the width of squared cross-section for each electrode is about 30μm, 600μm height and 70μm distance between neighbourhood electrodes were machined on high speed steel .Then 10×10 micro hole arrays were fabricated by 10×10 square micro electrode array of 40μm high by EMM, the diameter of single hole is about 100μm and deep is 30μm [31]. The possibilities in fabricating collective electrodes of various shapes by reverse EDM were discussed and in turn these collective electrodes were employed in machining micro hole arrays and grooves using micro ECM [32].

Peng et al. It was observed that, based on the principle of micro electrical discharge machining, a reversible machining method, which has capability to deposit metal material in order to develop of micro erections or pillars. As a result, a micro square column with 0.1mm in side length, 0.88mm in height and a micro pillar of 0.14mm in diameter, 1.18mm in height were developed [33]. A new EDM method of reversible machining for fabrication of micro-structures. It was suggested that this method was feasible for the fabrication of micro-structure with fine surface quality and high shape precision and can achieve the metal material depositing or removing in one EDM system to fabricate micro-structures by controlling the process. Micro-holes of diameter 80μm were made in the radial direction of the deposited steel cylinder and then an arrayed feature of 70μm in side length, a micro cylinder of diameter 135μm and height of 1445 μm were obtained successfully [34].

Liao et al. developed a method for machining high aspect ratio microstructure arrays by reverse Wire EDM. Machining was carried out by a micro brass wire of 20 μm to fabricate various high aspect ratio miniature structures including a microstructure array of 10 μm thickness and a microstructure array of 10×10 squared pillars [35].

2.2 Influence of process parameters and characteristics of textured surfaces

Singh et al. found that the electrodes fabricated from reverse EDM can be used in applications of micro ECM for the development micro holes arrays. It was further found the tapering of arrayed structures when there was increase in machining time and capacitance beyond 650 pF. In order to minimize the taper, usage of dual disk-type electrodes (Fig. 2.4) were machined by which dual micro structures can be developed with minimum taper and also increased the productivity of the process [32].
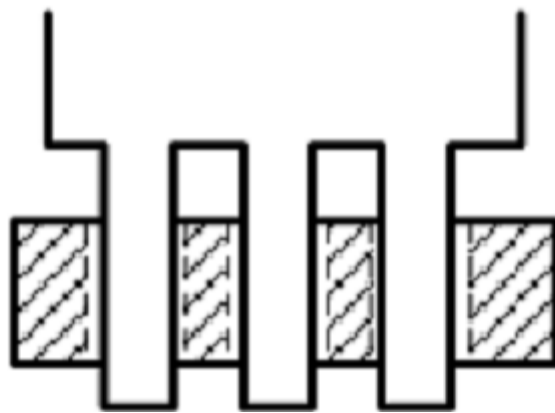
Fig. 2.4 Machining of disk type electrodes [32]

Joshi et al. investigated that capacitance and voltage were the significant processing parameters influencing the dimensional accuracy and surface finish of the arrayed structures. It was found that increase of pulse energy improved the dimensional accuracy and further investigated that voltage has highest effect compared to capacitance. At voltage of 80 V, because of repeated arcing and short weld establishment surface roughness of 3.5 µm was found on the structures as shown in Fig. 2.5. It also inferred that the higher pulse energies helps in improving the flushing action of the dielectric fluid to flush away the debris particles from the machined surface and helps in improves erosion rates [19].
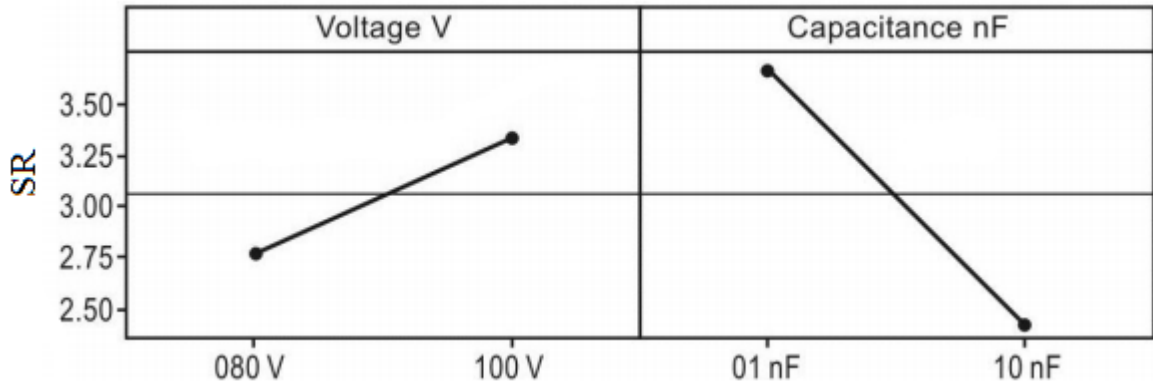
Fig. 2.5 Effect of voltage and capacitance on surface roughness [19]

Mastud et al. found the accumulation of debris particles in the inter-electrode gap (Fig. 2.6) during machining of high aspect ratio arrayed features and textured surfaces using R-MEDM process. It was suggested that vibration assisted R-MEDM can aid to overcome the concerns of debris accumulation and helps in development of debris free arrayed surface surfaces [36].Gap voltage, capacitance and feed rate were considered as the machining parameters in order to analyse material removal rate (MRR), surface roughness, surface integrity, dimensional accuracy of pillared structure. It was found that the MRR increased with supplied energy and a levelled surface with best mean dimensional accuracy was witnessed at 110V gap voltage and low capacitance. Surface morphology of the machined surface shows substantial surface impairment at 90 V [29].
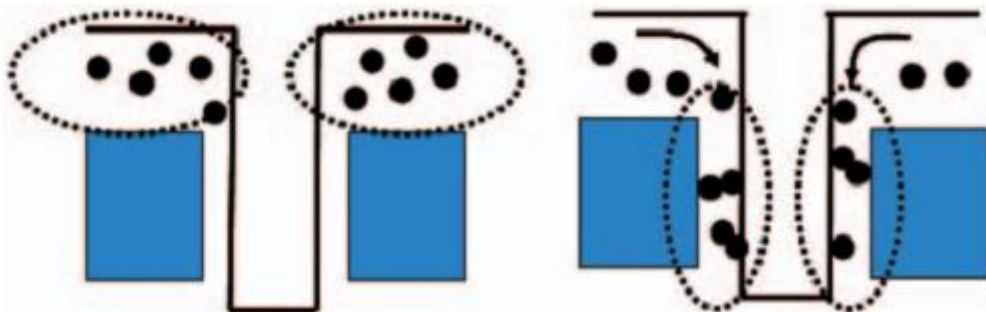
Fig. 2.6 Accumulation of debris particles in the electrode gap [36]

Hwang et al. analysed the influence of voltage, capacitance, amplitude and frequency of the anode (plate electrode) vibrations on the erosion rate and process stability during fabrication of textured surfaces. The process stability was measured in the percentages of the normal, open circuit and the short circuit durations in the voltage-current (V-I) signals during the process and observed increase of amplitude and the frequency of the vibrations with discharge durations [25].

Peng et al. studied the effect of various machining conditions such as open circuit voltage, discharge current, deposition rate and discharge on-time during deposition of microstructures using brass and steel as tool electrode and high speed steel as work piece. It was found that when discharge current was beyond 13 A the deposition process was failed and even the tool electrode was burnt. Similarly, when discharge on-time was above the value of 8 µs short circuit takes place which results in formation of less accurate structures [33].

CHAPTER 3

OBJECTIVE

It is evident from the past research work, EDM is an effective way for fabricating textured surfaces. Although some work has been reported on the development of arrayed structures or textured surfaces in form of micro protrusions using R-MEDM, sufficient information has not available in macro regime. There is no work related to aspects such as dimensional inaccuracies in the form of cylindricity error, degree of taper, surface integrity like surface roughness, micro hardness depth profiling and surface morphology of pillared structure.

.Therefore, the current study has been planned with the following objectives:

1. To develop array of pillared type structures using R-EDM which are typically utilized in the form of fins and in assembling operations.

2. To investigate the effect of various parameters such as peak current (I_p), pulse-on time (T_{on}) and flushing pressure (F_p) with the help of response surface methodology (RSM) based design experiments (DOE) on different performance measures such as material removal rate (MRR), surface roughness (SR), taper, cylindricity error and also micro hardness depth profiling and surface morphology of pillared structure during R-EDM of mild steel.

3. To optimize the various performance measures during R-EDM process using a hybrid approach of grey relational analysis (GRA) in combination with principal component analysis (PCA) and thus to obtain the optimum process parameter combination which can yield the best output response characteristics.

CHAPTER 4

EXPERIMENTAL PROCEDURE

4.1 Experimental setup

For fabricating arrayed structures, the whole experimentation was carried out on die sinking EDM (model: ELECTRONICA –ELECTRAPLUS PS 50ZNC) as shown in Fig. 4.1. The tool electrode used for the experiment was made from square copper plate of cross sectional area 25×25 mm^2 which acts as cathode and mild steel was used as a work piece, acts as anode. A servo controlled mechanism was used to maintain constant gap between anode and cathode called inter electrode gap. The electrodes are immersed in a dielectric fluid called EDM oil (Freezing point = 94℃, specific gravity = 0.763).

Fig. 4.1. Experimental setup

4.2. Tool Design

The electrode (cathode) for the fabrication of arrayed structures was prepared from the copper plate of area 25×25 mm^2. An array of 3×3 holes (depth 2mm and Ø3mm) i.e. three holes in each row with a gap of 5mm were drilled using a drill bit of Ø3mm on CNC milling machine as shown in Fig. 2. After that, a shank of length 6mm and Ø10mm brazed to the copper plate using borax as flux powder. The design of tool is showed in Fig. 4.2
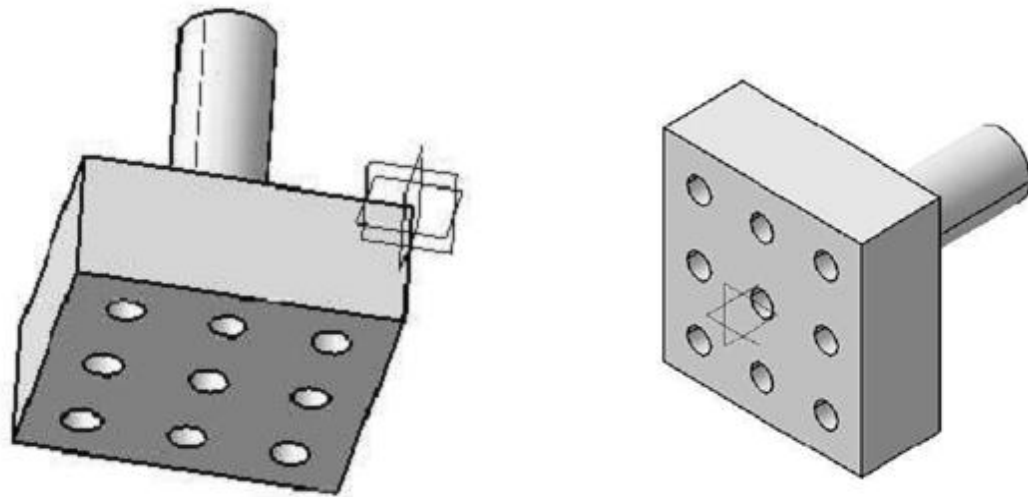
Fig. 4.2 Design of Cu tool with 3×3 array of holes

When the electrode is fed against the work piece (anode) at a controlled rate, selective material removal takes place from work piece surface and at the surface of the anode having interface with cavities on cathode no erosion takes place and appears as raised structures. Thus, the pattern of cavities from cathode is replicated to the work piece surface. Fig. 4.3 represents copper tool with array of holes and Fig. 4.4 indicates work piece with array of structures.

| Fig. 4.3. Cu tool with array of holes | Fig. 4.4 Work piece with arrayed structures |

4.3. Design of Experiments using RSM

RSM is a group of mathematical and statistical techniques that are worthwhile for modelling and investigation of problems in which a number of variables effects a response of concern and objective is to optimize this response. It is one of the Design of Experiments (DOE) techniques employed to estimate an unknown equation for which only a few responses are calculated. A Central Composite Design (CCD) is utilized as it provides reasonably precise estimate of all response variables. The benefit of CCD is that it allows acceptable level adjustments. In these techniques, there is a prospect that after few experimental runs it stops and decides that the estimated model is acceptable [37].

In order to understand the influence of factors on the above stated machining conditions, second order polynomial response surface mathematical models can be developed. In general, the response surface is described by an equation as

$$Y = c_0 + \sum_{i=0}^{n} c_i x_i + \sum_{i=0}^{n} c_i x_i^2 + \sum_{i<j=0}^{n} d_i x_i x_j \pm \delta_r \qquad (1)$$

Where Y is the corresponding response, X_i refers to the input variables, X_i^2 and X_iX_j are the squares and interaction terms respectively of these input variables. C_0, C_i and d_i are unknown regression coefficients and δ_r indicates random error.

In the current study, the machining was done by choosing peak current (I_p), pulse-on time (T_{on}) and flushing pressure (F_p) as input parameters and the other parameters such as duty factor (τ_{au}) equal to 80 % and gap voltage of 50 V are kept constant throughout the experiment.

The values of control parameter and their levels are shown in Table 4.1.

Table 4.1 Machining parameters and their levels

Level	Experimental control factors		
	Peak current(I_p) (A)	Pulse-on time (T_{on}) (μs)	Flushing pressure(F_p) (Kg/cm^2)
1	10	100	0.2
2	12	200	0.24
3	15	300	0.30
4	18	400	0.36
5	20	500	0.4

4.4 Measurement of responses

For fabricating arrayed structures, the output responses such as MRR, SR, taper, cylindricity and micro hardness were measured. The measurement approach of these output responses were discussed as below.

MRR is defined as the ratio of the difference of weight of the work piece before and after machining to the machining time and density of the material as shown in Eq. 2.

$$MRR = \frac{W_i - W_f}{D \times t} \ mm^3/min \qquad (2)$$

Where, W_i, weight before machining (gm), W_f weight after machining (gm), D is density of work piece material (gm/mm^3) & t is the time consumed for machining (min).

Surface roughness can be defined as the unevenness of the machined surface. In this study, Surface roughness (R_a) was measured by portable type profilometer i.e. Talysurf (Model: Taylor Hobsonsurtronic3+).For a particular work piece, a set of four readings were measured and average of these values has been considered for analysis.

For the measurement of taper angle, a set of six readings were taken for each work piece using optical microscope of magnification of 25X (Table 3) as shown in Fig. 3 and angle has been measured using the following Eq. 3

$$\tan\theta = \frac{(D-d)}{2 \times h} \tag{3}$$
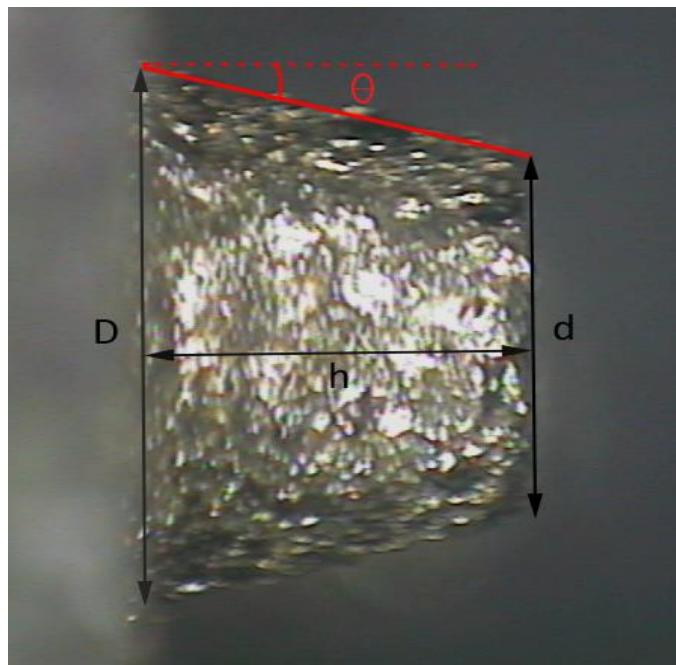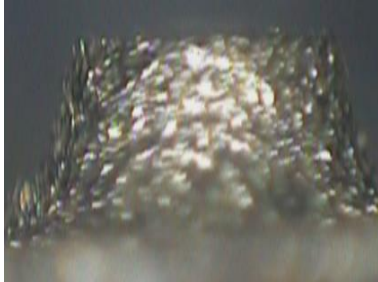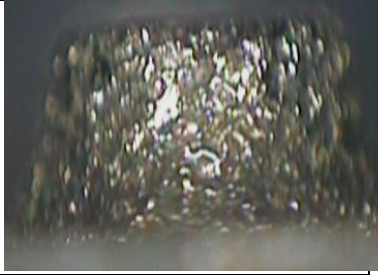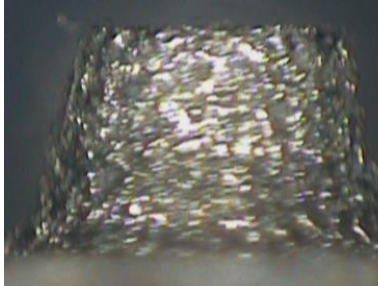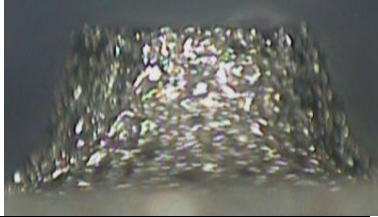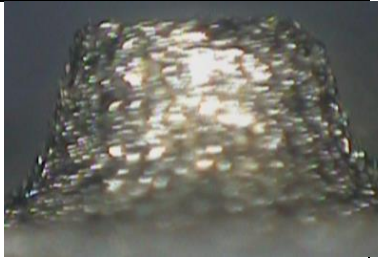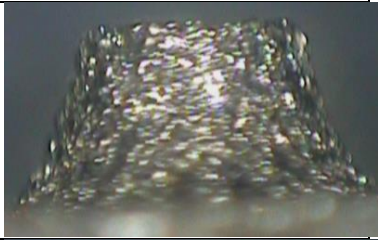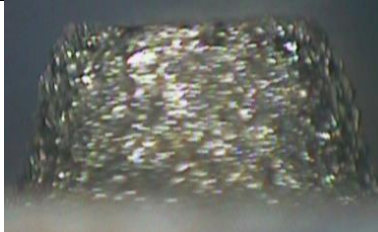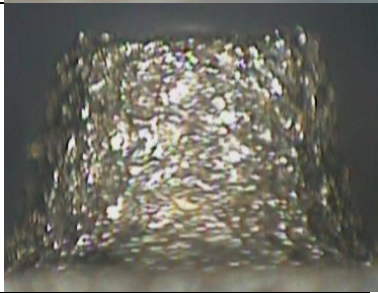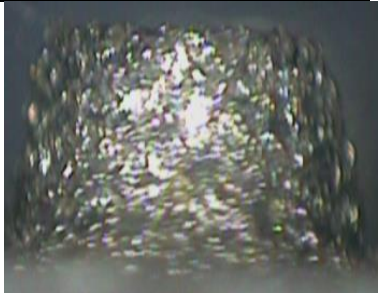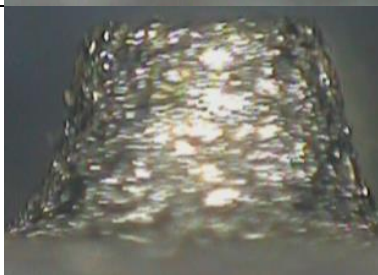
Fig. 4.5 taper angle measurement of arrayed structure

Where'd' is the upper diameter and 'D' is the lower diameter of projection respectively and 'h' is taper length.

Table 4.2 Microscopic images for measuring taper

S.no	parameters	Microscopic images for measuring taper
1	$I_P = 10$ A $T_{on} = 300$ μs $F_p = 0.3$ kg/cm^2	
2	$I_P = 12$ A $T_{on} = 200$ μs , $F_p = 0.24$ kg/cm^2	
3	$I_P = 12$ A $T_{on} = 200$ μs , $F_p = 0.36$ kg/cm^2	
4	$I_P = 12$ A $T_{on} = 400$ μs $F_p = 0.36$ kg/cm^2	
5	$I_P = 15$ A $T_{on} = 300$ μs $F_p = 0.2$ kg/cm^2	

6	$I_P = 15$ A $T_{on} = 300$ μs $F_p = 0.3$ kg/cm^2	
7	$I_P = 15$ A $T_{on} = 300$ μs $F_p = 0.4$ kg/cm^2	
8	$I_P = 15$ A $T_{on} = 500$ μs $F_p = 0.3$ kg/cm^2	
9	$I_P = 18$ A $T_{on} = 200$ μs $F_p = 0.24$ kg/cm^2	
10	$I_P = 18$ A $T_{on} = 200$ μs $F_p = 0.36$ kg/cm^2	
11	$I_P = 18$ A $T_{on} = 400$ μs $F_p = 0.24$ kg/cm^2	
12	$I_P = 18$ A $T_{on} = 400$ μs $F_p = 0.36$ kg/cm^2	

Cylindricity error is the difference between measured cylindrical surface and its ideal cylindrical surface. It is a significant quality index that indicates the precision of mechanical parts and assembled parts [38]. The value of cylindricity error has great influence on wear resistance, rotation and assembly accuracies of machined parts .In our present study cylindricty error of arrayed structures was measured with the help of coordinate measuring machine (CMM) as shown in Fig. 4 by taking a set of four readings along the longitudinal axis of protrusions for each work piece.
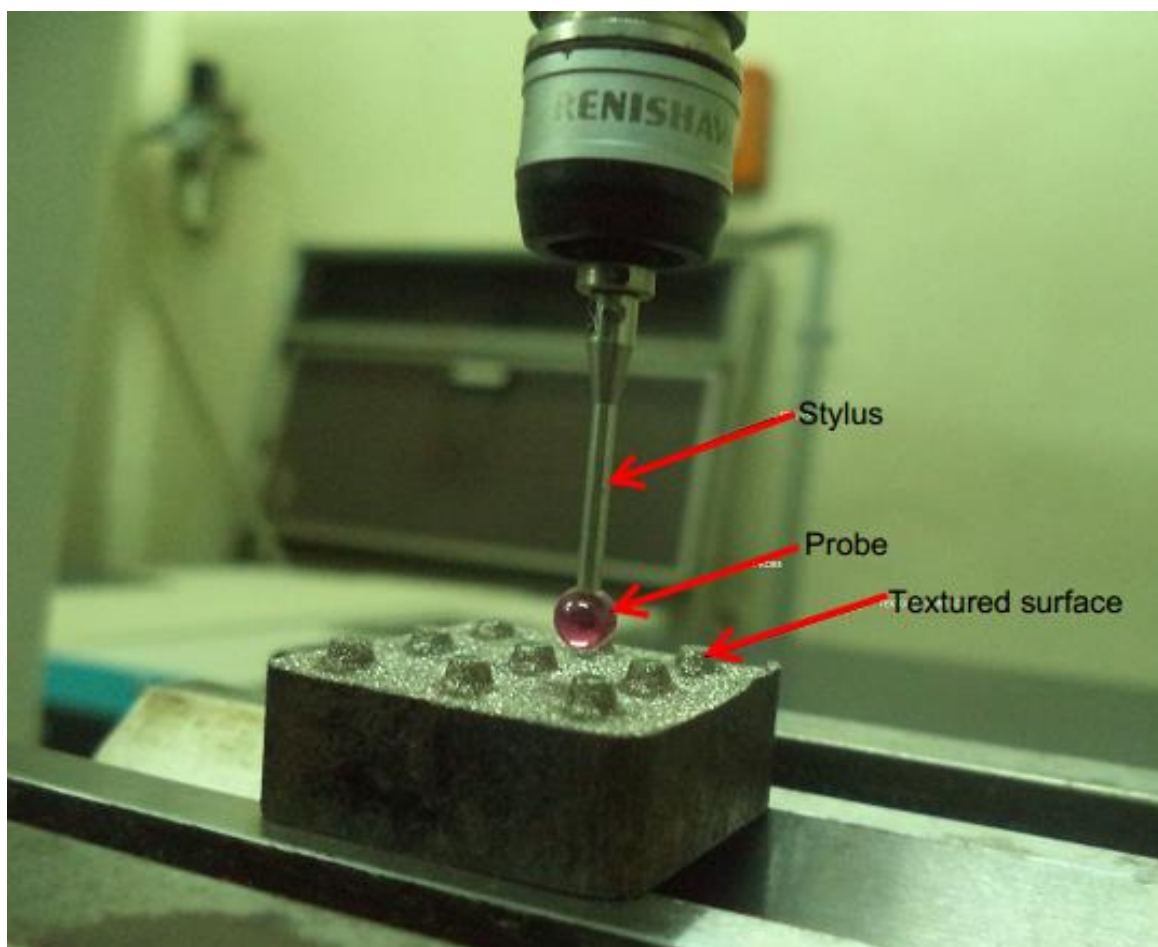
Fig. 4.6 Measurement of cylindricity error using CMM

4.5 Grey PCA analysis

It is essential for any method to determine optimal combination of process parameters to yield best output responses. Therefore, in order to determine the influence of multiple parameters on various responses, a multi-objective optimization must be applied to achieve an optimal parameter combination. Numerous optimization strategies have developed throughout these years to solve problems involving number of input parameters. One such technique is principal component analysis based grey analysis. PCA based grey analysis is a normalization technique useful in converting multiple responses into unique characteristic index known as overall quality performance index (OQPI) [39].

Grey relational analysis coupled with principal component analysis (PCA) was used for obtaining optimal process parameters to fabricate arrayed features during reverse EDM of mild steel. The procedure for Grey PCA was explained as below

In this method, firstly the output responses are converted to S/N ratios.

The S/N ratios are fundamentally of three types lower-the-better (LTB), higher-the-better (HTB) and nominal-the-better (NTB). In this analysis we utilized the S/N ratio with LTB and HTB represented by the following equations.

Lower the better Response variable

$$\rho_{ij} = -10 \log \left[\frac{1}{N} \Sigma_{K=1}^{N} y_{ijk}^{2} \right] \tag{4}$$

Higher the better response variable

$$\rho_{ij} = -10 \log \left[\frac{1}{N} \Sigma_{K=1}^{N} y_{ijk}^{-2} \right] \tag{5}$$

Where N = number of repetitive trials y_{ijk} = experimental data of jth response in i^{th} experiment at k^{th} repetition. Now, by utilizing these S/N ratio the Principal component scores (PCS) to each experimental run can compute by the following equation

$$X_i(n) = a_{11}\omega_{11} + a_{22}\omega_{22} + \cdots\cdots\cdots a_{ij}\omega_{ij} \tag{6}$$

Where $X_i(n)$ represents PCS of ith factor in n^{th} experimental run and $\omega_{11,}\omega_{22,}\cdots\cdots\omega_{ij}$ are the eigen vectors corresponding to n^{th} eigen value of each response which can be evaluated by MINITAB software.

The PCSs so obtained are normalized as follows

The response characteristics having higher the better characteristic normalized by the following equation

$$Z_i^*(n) = \frac{X_i(n) - \min X_i(n)}{\max X_i(n) - \min X_i(n)} \tag{7}$$

The sequence having lower the better characteristic is normalized as follows

$$Z_i^*(n) = \frac{\max X_i(n) - X_i(n)}{\max X_i(n) - \min X_i(n)} \tag{8}$$

Where, i=1,2…..m; n=1,2,….p; m represents total experimental runs and p indicates number of performance characteristics; $\min X_i(n)$ and $\max X_i(n)$ are the minimum and maximum values of the initial sequence respectively. $Z_i^*(n)$ is the obtained value after normalization of n_{th} element in the i_{th} sequence.

After normalizing the sequences, the grey relation coefficient (GRC) is calculated. The grey relational coefficient (GRC) can be calculated by using following expression.

$$\Delta_i(n) = \frac{\alpha_{min} + \gamma\alpha_{max}}{\alpha_{0,i}(n) + \gamma\alpha_{max}} \tag{9}$$

Where γ is the identification coefficient which is normally taken in the range [0, 1] [40]. In our analysis γ is taken as 0.5 and α_{min} and α_{max} are the global minimum and global maximum values of the normalized sequences.

$$\alpha_{0,i}(n) = \left| Z_0^*(n) - Z_i^*(n) \right|$$, is called the deviation sequence.

Where $Z_0^*(n)$ represents the reference sequence and $Z_i^*(n)$ represents the comparability sequence.

Finally, calculation of OQPI .In real engineering problems, the effect of various input variables on the output response varies. Hence, there arises a need to allocate a weighting factor to the grey coefficients for evaluation of OQPI. Mathematically, OQPI is calculated as a sum of the weighted grey relational coefficients and it is represented as

$$\delta_i = \frac{1}{N} \sum_{i=1}^{p} \beta_{ni} \, \Delta_i(n) \tag{10}$$

Where β_{in} is the weightage given and $\sum_{i=1}^{p} \beta_{ni} \, \Delta_i(n) = 1$ Basically OQPI indicates the amount of influence exerted by the comparability sequence over the reference sequence.

In general, a set of input factors correspond to high OQPI value means it has highest influence on performance characteristics.

CHAPTER 5

RESULTS AND DISCUSSIONS

After machining, output characteristics were calculated and depicted in Table 5.1

Table 5.1 Experimental Results

S.no	I_p (A)	T_{on} (µs)	F_p (kg/cm^2)	MRR (mm^3/min)	SR(R_a) (µm)	Taper (degree)	cylindricity error (mm)
1	15	300	0.3	43.94	8.2	12.61	0.3497
2	18	200	0.36	60.154	10.5	15.145	0.4228
3	12	400	0.36	36.099	7.25	10	0.2597
4	15	300	0.3	47.144	8.8	11.89	0.3389
5	12	200	0.24	41.147	7.68	9.62	0.2248
6	18	400	0.24	55.949	11.35	14.74	0.4162
7	18	200	0.24	62.622	10.25	14.52	0.4211
8	15	300	0.3	46.963	8.45	11.34	0.3564
9	18	400	0.36	60.518	12.7	14.86	0.3418
10	12	200	0.36	40.583	7.55	9.51	0.2367
11	15	300	0.3	44.704	8.3	12.53	0.3458
12	12	400	0.24	34.98	7.2	10.17	0.232
13	20	300	0.3	68.089	13	16.65	0.2158
14	15	100	0.3	50.33	7.9	12.05	0.3638
15	15	300	0.2	45.245	8.4	13.12	0.3122
16	10	300	0.3	24.76	6.8	10.24	0.1287
17	15	500	0.3	42.679	8.1	13.02	0.3715
18	15	300	0.3	43.091	8.25	11.66	0.3108
19	15	300	0.4	47.245	8.45	12.36	0.3494
20	15	300	0.3	43.119	8.75	11.95	0.3211

5.1. Analysis of effect of various machining conditions on output responses through RSM based surface plots

5.1.1 Influence of process parameters on MRR

(a)

(b)

(c)

Fig. 5.1 Surface plots showing the variation of MRR with respect to the combined effect of (a).T_{on} and I_p (b). I_P and F_p (c).T_{on} and F_p

Table 5.2 ANOVA analysis of MRR

Source	DOF	Sum of squares	Mean square	P value	% of contribution
I_p	1	1856.77	1856.77	0.000	93.49
T_{on}	1	65.06	65.06	0.009	3.28
F_p	1	2.62	2.62	0.526^*	0.132
Residual error	10	61.45	6.15	-	3.094
Total	16	1985.9	-	-	100

* indicate non-significant

The response surface plots for MRR in relation to process parameters I_p and T_{on} and F_p. From the Fig. 5.1, we infer that MRR increases significantly with increase in I_p for any value of T_{on} due to dominant control over spark energy. However, MRR tends to increase with T_{on}, especially at higher values of I_p due to large impulsive force in the electrode gap. Hence, maximum MRR is obtained at a peak current of 20 A and pulse-on time of 500µs. Also from ANOVA Table 5.2. it can confirm that peak current and pulse-on time are the dominant factors It is observed that MRR values are high at high flushing pressures and low pulse-on time values. This is because at low pulse-on times impetuous power in spark gap is less that allows the dielectric fluid to remove the previously accumulated debris effectively.

The effect of different process parameters on MRR was mathematically formulated in form of Eq. 11

$$\text{MRR} = 44.8275 + (19.506 * I_p) - (4.03275 * T_{on}) + (0.7364 * F_p) + (3.4143 * I_p^2) + (3.48646 * T_{on}^2) + (3.2348 * F_p^2) \tag{11}$$

5.1.2. Influence of process parameters on surface roughness

Fig.5.2. Surface plots showing the variation of R_a with respect to the combined effect of

(a).T_{on} and I_p (b). I_P and F_p (c). T_{on} and F_p

Table 5.3 ANOVA analysis of R_a

Source	DOF	Sum of squares	Mean square	P value	% of contribution
I_p	1	47.7938	47.7938	0.000	91.97
T_{on}	1	0.5402	0.5402	0.092*	1.039
$I_p \times T_{on}$	1	2.0808	2.0808	0.004	4.004
Residual error	10	1.5518	0.1552	-	2.986
Total	16	51.9666	-	-	100

* indicate non-significant factors

Since material removal in EDM is achieved through the formation of craters due to sparks, it is obvious that large craters results in rough surface, so crater size and the quality of surface depends mainly on energy per spark. It believed that a pool of molten metal develops in machined zone due to increase in peak current, which evaporates, and so forming bubbles explodes when discharge takes place leaving craters on the surface. Like that, successive discharge will result in crater and pockmarks thus increasing R_a the same can be seen from Fig. 5.2. With increase of T_{on} R_a first increases and then decreases with T_{on}, because as T_{on} increases energy density decreases. R_a has minimum value at low current and moderate flushing pressure because of low spark energy and efficient removal of debris. From ANOVA Table 5.3 we can figure out that peak current has highest contribution on R_a followed by I_P and T_{on} interaction. The predicted mathematical model for R_a was shown in the Eq. 12

$$R_a = 8.47 + (1.86*I_p) + (0.22*T_{on}) + (0.12*F_p) + (0.61*I_p^2) - (0.094*T_{on}^2) + (0.088*F_p^2) \quad (12)$$
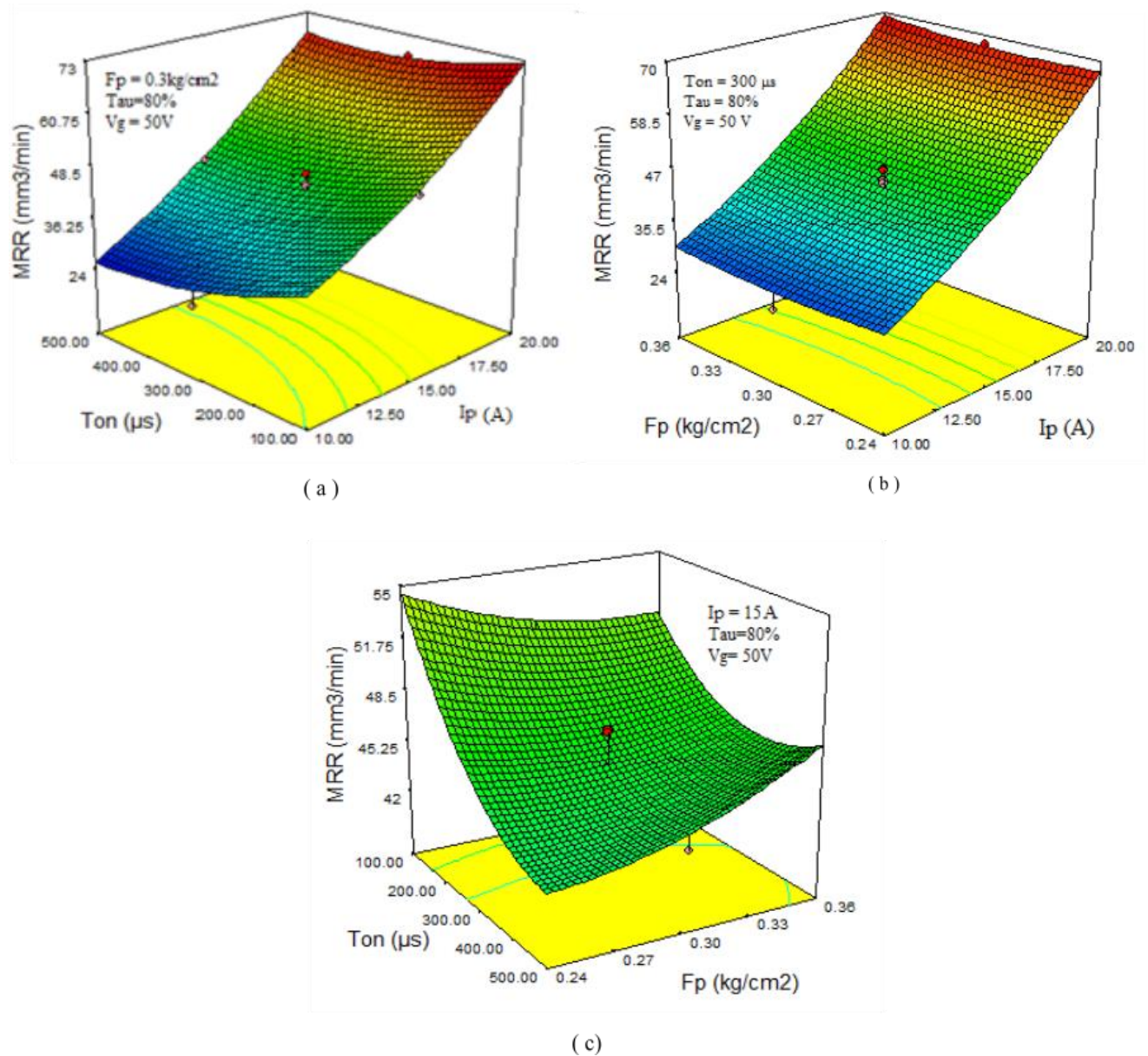
5.1.3. Influence of process parameters on taper
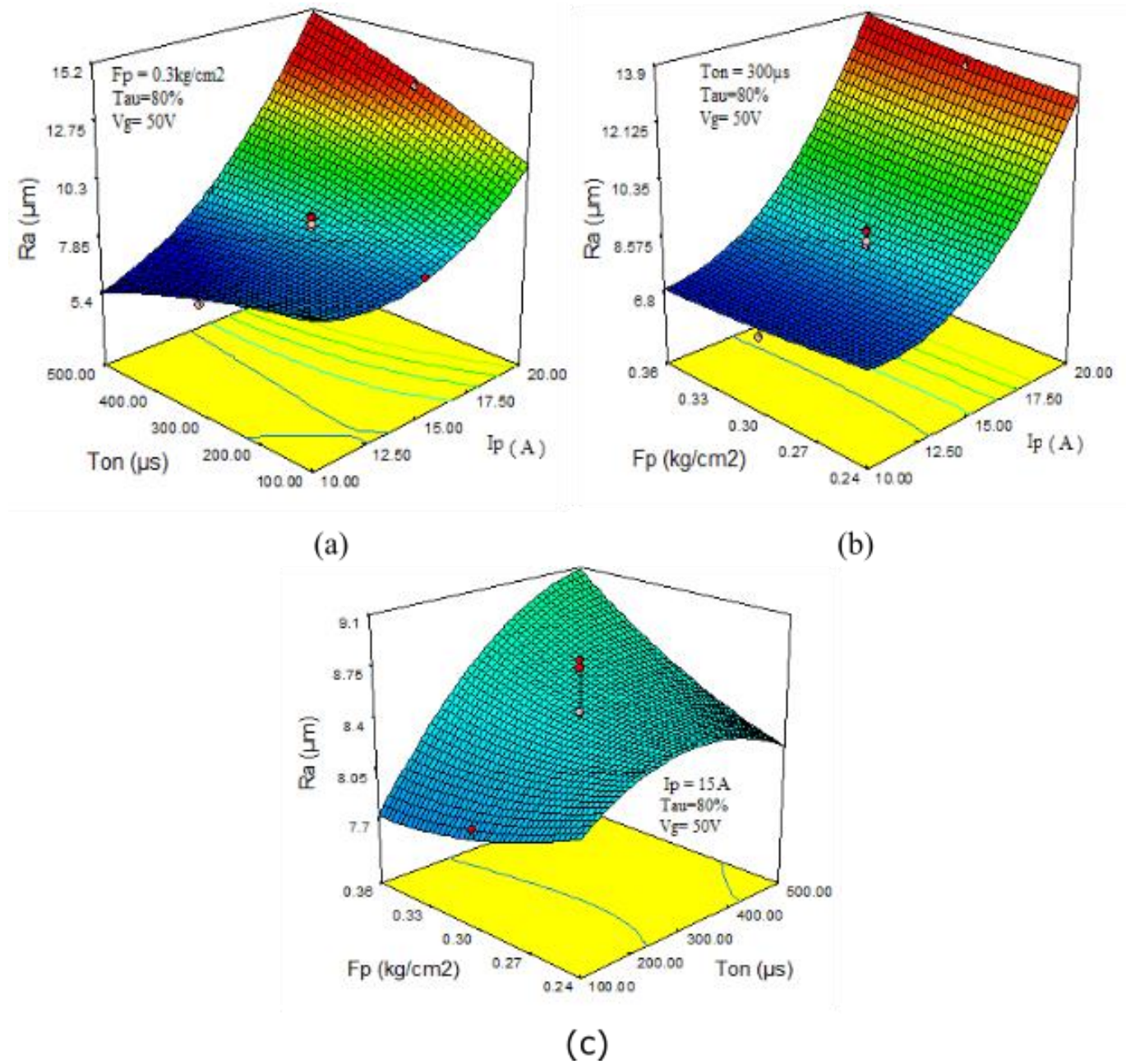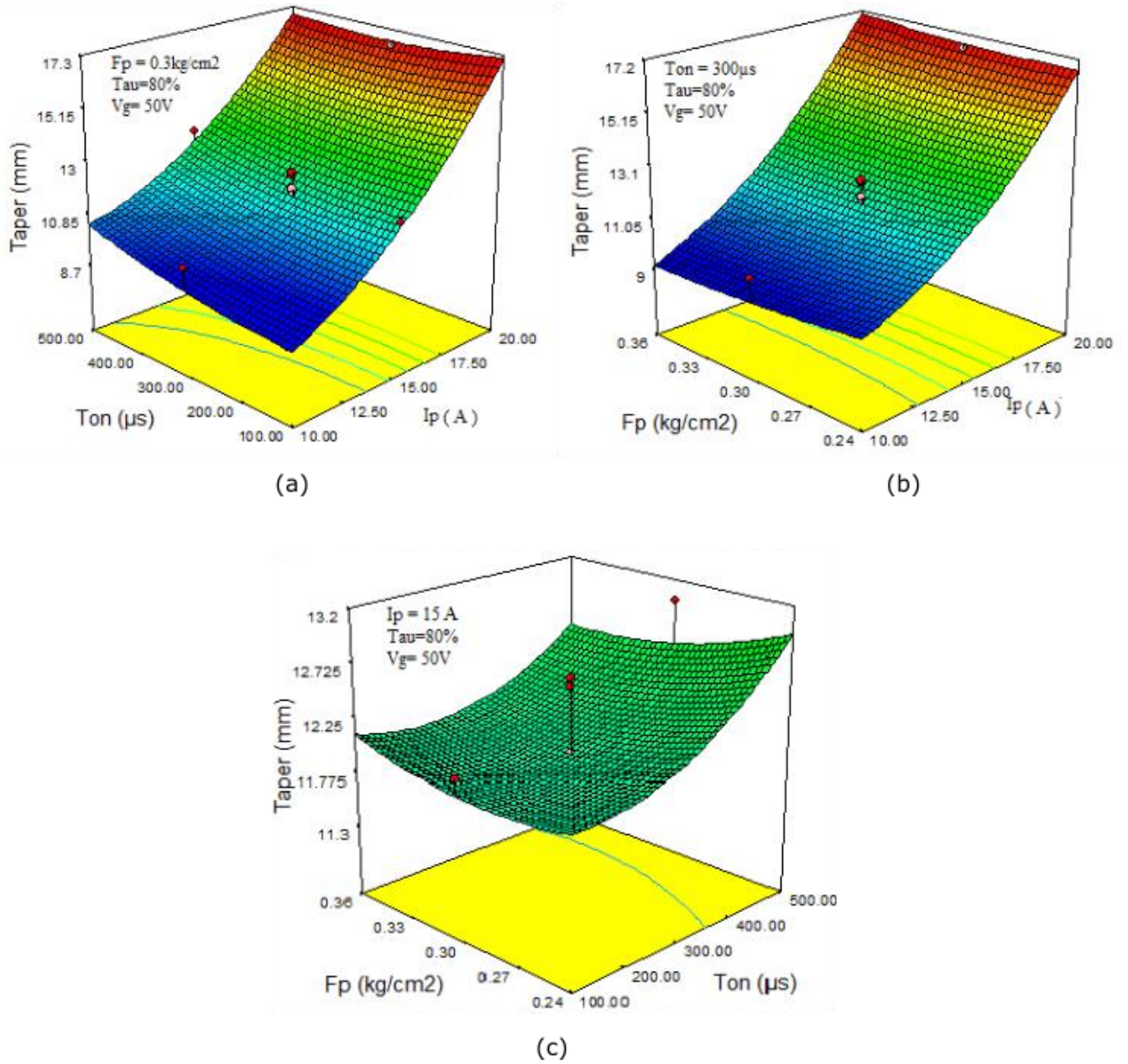

Fig. 5.3 Surface plots showing the variation of taper with respect to the combined effect of (a). T_{on} and I_p (b) I_p and F_p (c). T_{on} and F_p

Table 5.4 ANOVA analysis of taper

Source	DOF	Sum of squares	Mean square	P value	% of contribution
I_p	1	69.2941	69.2941	0.000	93.927
T_{on}	1	0.5311	0.5311	0.27*	0.7198
F_p	1	0.0474	0.0474	0.735*	0.0642
Residual error	10	3.9024	0.3902	-	5.289
Total	16	73.775	-	-	100

* indicate non-significant factors

Tapering of textured surfaces results because the upper portion of hole walls is subjected to more number of sparks than bottom portion. It is observed that with increase in peak current and pulse-on time, the taper angle subsequently increases. From response surface plots (i.e. Fig. 5.3) and from Table 5.4, it is found that the peak current is the most significant one. The dependency of the taper angle on the dielectric flushing pressure is comparatively less significant. As the material removal takes place, the spark gap simultaneously increases throughout the process. At a given feed rate of the tool, the upper part of the work piece is more eroded than the lower part. This gives rise to linearly decreasing spark gap from the top of the work piece until the bottom, which is viewed as linear taper on the work piece. Therefore, with higher rate of material removal, the tapering is more. Fig. 5.4 shows variation in taper of arrayed structures at different input conditions.

I_p=15 A,T_{on}=300 μs, F_p= 0.2 kg/cm² I_p=18 A,T_{on}=200 μs, F_p= 0.36 kg/cm²
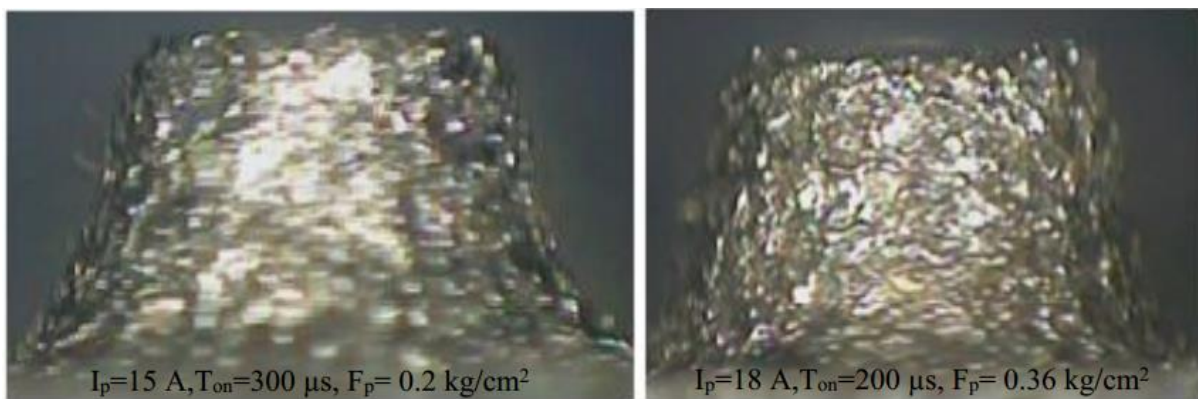
Fig.5.4 Microscopic images of taper of arrayed structures at different parametric combination

The mathematical model for taper relating input parameters and output responses is formulated in the form of Eq. 13.

$$\text{Taper} = 11.9923 + (3.7682*I_p) + (0.36437*T_{on}) - (0.09856*F_p) + (1.0578*I_p^2) +$$
$$(0.1957*T_{on}^2) + (0.3525*F_p^2)$$

$$(13)$$

5.1.4. Influence of process parameters on cylindricity error

(a)

(b)

(c)
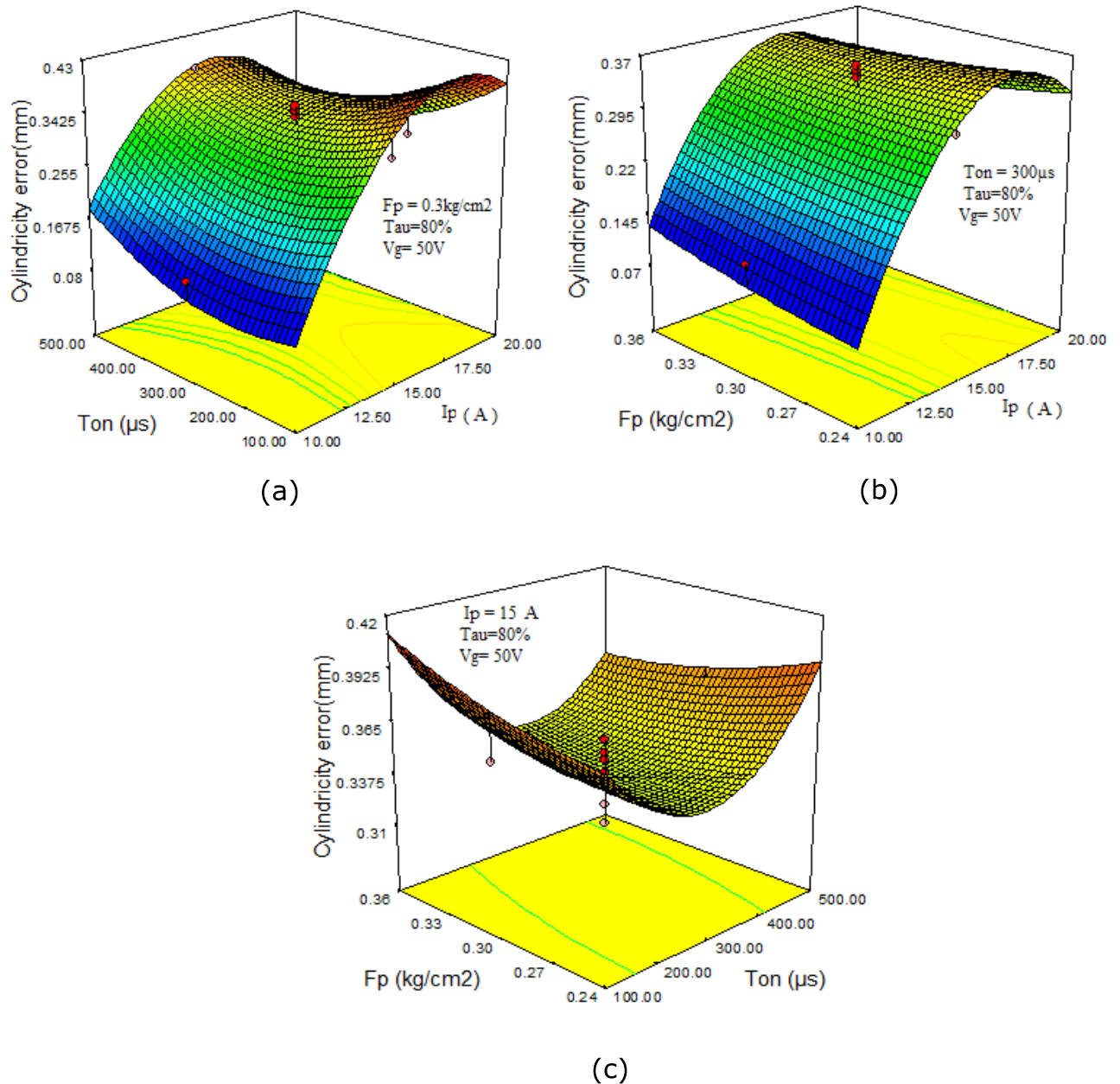
Fig. 5.5 Surface plots showing the variation of cylindricity error with respect to the combined effect of   (a).T_{on} and I_p (b). I_P and F_p (c). T_{on} and F_p

Table 5.5 ANOVA analysis of cylindricity error

Source	DOF	Sum of squares	Mean square	P value	% of contribution
I_p	1	0.046492	0.046492	0.000	43.65
T_{on}	1	0.000102	0.000102	0.818*	0.0958
$I_p \times I_p$	1	0.041728	0.036378	0.001	39.174
Residual error	10	0.018198	0.001820	-	17.084
Total	16	0.10652	-	-	100

* indicate non-significant factors

From response surface plots (Fig. 5.5), and from ANOVA Table 5.5, it was found that the peak current is the dominant factor that controls the cylindricity profile of the arrayed structures. cylindricity error first increases with Ip and then falls since as the current and pulse-on time increases the MRR is so high that the machined surface takes exactly the shape of tool so that the projections erected are very straight and it results in little deviation from ideal cylindrical shape. Similarly as the flushing pressure increases we observed the same trend since with high dielectric pressure the molten material flushes away from the machined surface allowing the tool to erode the work piece to its full depth resulting in minimum cylindricity error.

The mathematical model for cylindricity error was given by Eq. 14

$$\text{Cylindricity error} = 0.34 + (0.058 * I_p) - (2.995\text{E-}003 * T_{on}) + (2.113\text{E-}003 * F_p) - (0.05 * I_p^2) + (0.016 * T_{on}^2) + (5.612\text{E-}003 * F_p^2) \tag{14}$$

5.1.5 Micro hardness depth profiling

(a)   (b)
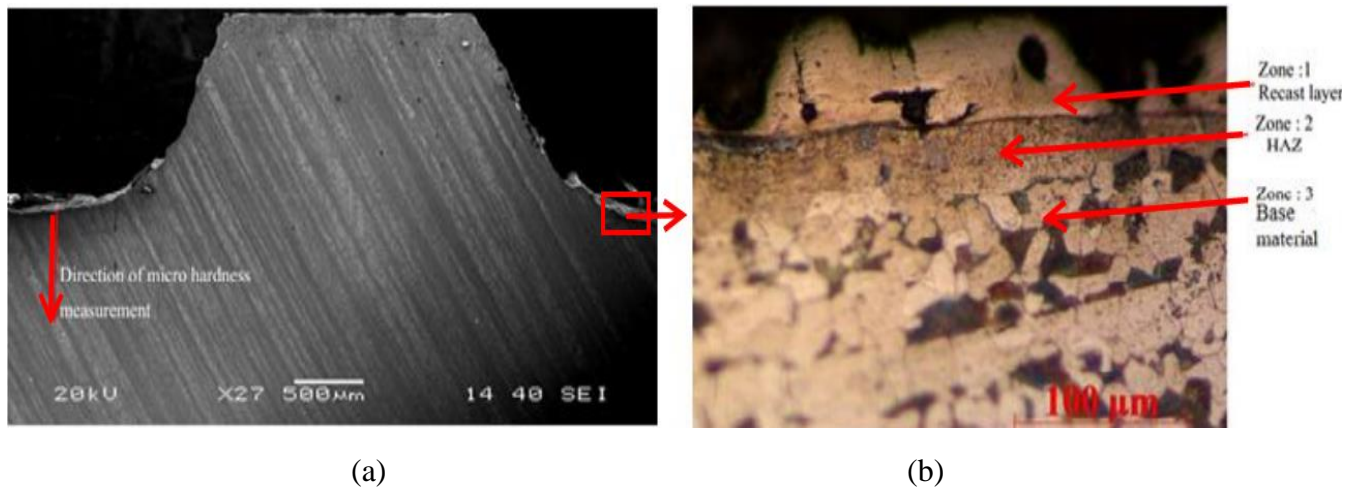
Fig. 5.6 (a) SEM image showing the cross-section of pillared structure (b). Microscopic image showing three distinct zones in cross-section of pillared structure

The cross-section of the pillared structure was polished and then etched with NITAL (ethanol and nitric acid) etchant. After etching the cross-section revealed three different zones which include recast layer, heat affected zone (HAZ) and base material as shown in Fig. 5.6(b). With increase of peak current the recast layer subjected to thermal softening due to increase in discharge energy. Hence micro hardness is less in this region. The layer beneath the recast layer called heat effected zone (HAZ) is subjected to severe heating and quenching which results in higher micro hardness in this region. Further below the HAZ, micro hardness tends to decrease and reaches the base material.

(a)

(b)

(c)
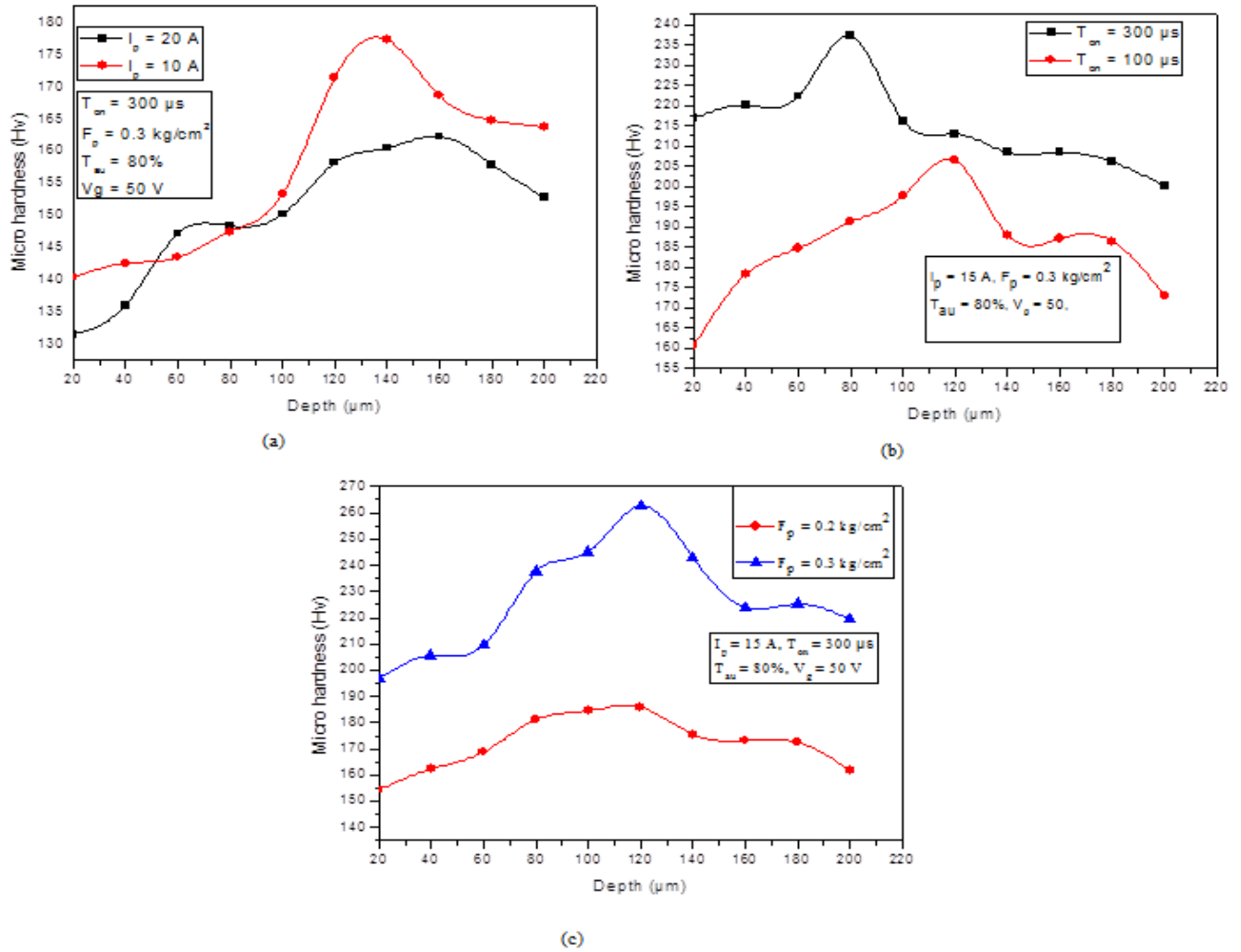
Fig. 5.7 Variation of micro hardness with (a) I_p (b) T_{on} and (c) F_p

Since the cross-section consists of three distinct layers, micro hardness of surface and sub-surface was evaluated with the help of Vicker's micro hardness tester. The test was carried out at various depths starting from surface and then gradually moved deep inside towards the base material as shown in Fig. 5.6 (a).Further the variation of micro hardness of surface and sub-surface with respect to various parameters were discussed.

From Fig. 5.7(a) it was observed that micro hardness is high at peak current (I_p) of 10 A when compared to I_p at 20 A. This is due to high thermal softening effect at large I_p values. An increase in micro hardness is observed in Fig. 5.7 (b) with the increase in T_{on} from 100 μs to 200 μs due to the decrease in discharge density. Micro hardness improved with the rise of

flushing pressure from 0.2 kg/cm^2 to 0.3 kg/cm^2. At high flushing pressure EDM process becomes unstable due to the turbulence in inter electrode gap, particularly in surface texturing. This phenomenon prevents proper melting and solidification of work piece material resulting in high micro hardness.

5.1.6 Surface morphology of pillared structure
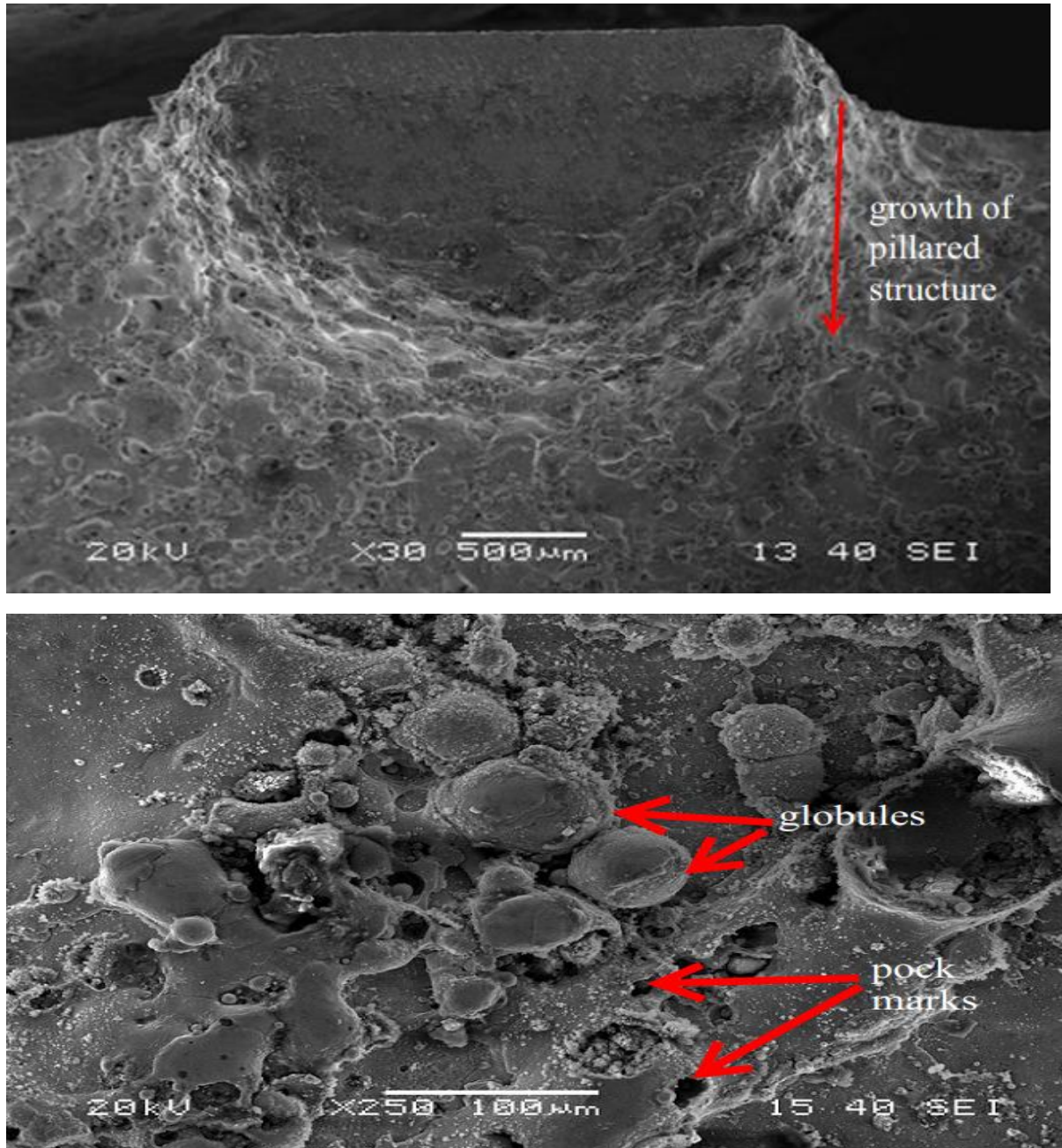
Fig. 5.8 SEM image showing surface morphology of pillared structure

Fig. 5.8 shows the top surface morphology and also surface morphology of pillared structure. It is evident that how growth or development of pillar takes place during R-EDM process. If the surface of the pillared structure was further magnified, surface contains impurities such as globules and pock marks.

5.2 Principal component analysis (PCA) based grey relational analysis (GRA) optimization for the determination of optimal machining parameters

The procedure for the Grey PCA optimization is described in the following steps

1. Convert output responses from the experimental data into signal- to -noise (S/N) ratios.

2. Calculate the principal component scores (PCS)

3. Normalization of PCSs and calculation of Grey relation coefficient for these normalized values.

4. Finally calculate OPQI

The output responses measured after the experiment listed in the Table 5.1 were converted into their respective S/N ratios using Eq. (4) and (5) respectively and the same were shown in Table 5.2. In this study, the response MRR was taken as the 'HTB S/N ratio' whereas for the responses SR, taper and cylindricity error 'LTB S/N ratio', after that principal component scores (PCS) for each run evaluated using Eq. (6). and the corresponding eigen values and eigen vectors for the output responses were calculated using MINITAB software.

Now PCSs of output responses so obtained were normalized i.e. MRR having 'larger-the-better' characteristic was normalized with the help of the Eq. (7) and likewise surface roughness, taper and cylindricity error having 'smaller-the-better' characteristic were normalized using Eq. (8) and are tabulated in Table 5.3.

Table 5.6 S/N ratio sequence of output responses

Run no.	MRR (mm³/min)	cylindricity error (mm)	Taper (degree)	Surface roughness (μm)
1	32.8572	9.126087	-22.0143	8.2763
2	35.58529	7.4773	-23.6054	-20.4238
3	31.1499	11.71056	-20	-17.2068
4	33.46853	9.398569	-21.5036	-18.8897
5	32.28676	12.96407	-19.6635	-17.7072
6	34.95585	7.613958	-23.3699	-21.0999
7	35.93454	7.512295	-23.2393	-20.2145
8	33.43512	8.961246	-21.0923	-18.5371
9	35.63769	9.324559	-23.4404	-22.0761
10	32.16688	12.51603	-19.5636	-17.5589
11	33.00693	9.2235	-21.959	-18.3816
12	30.8764	12.69024	-20.1464	-17.1466
13	36.66154	13.31897	-24.4283	-22.2789
14	34.03654	8.782746	-21.6197	-17.9525
15	33.11141	10.11134	-22.3587	-18.4856
16	27.87501	17.80843	-20.206	-16.6502
17	32.60428	8.600824	-22.2922	-18.1697
18	32.68773	10.15038	-21.334	-18.3291
19	33.48712	9.133542	-21.8404	-18.5371
20	32.69337	9.867194	-21.5474	-18.8402

Table 5.7 Normalized sequences of the response characteristics

Run no.	MRR (mm³/min)	cylindricity error (mm)	Taper (degree)	Surface roughness (μm)
1	0.341751	0.921453	0.368551	0.374435
2	0.004544	0.940417	0.625132	0.423341
3	0.636628	0.734831	0.555559	0.305738
4	0.319368	0.867759	0.688249	0.296278
5	0.62056	0.56115	0.970734	0.570813
6	0.018518	0.888141	0.608327	0
7	0.014883	0.962478	0.781363	0.541998
8	0.339232	0.958459	0.746286	0.286528
9	0	0.61295	0.8727	0.09831
10	0.621724	0.629401	0.943263	0.512667
11	0.336184	0.904892	0.426398	0.385203
12	0.677558	0.611397	0.492388	0.403232
13	0.035226	0.071342	1	1
14	0.308569	1	0.685596	0.709089
15	0.339201	0.77436	0.385609	0.558181
16	1	0	0	0.429122

17	0.328163	0.983351	0.213715	0.311272
18	0.41048	0.814246	0.554591	0.344355
19	0.310231	0.911169	0.567573	0.436567
20	0.36977	0.809915	0.526512	0.165881

The deviation sequences were then calculated and the values were then used to calculate grey relation coefficient using Eq. (9). and shown in Table 10. Finally, OQPI for each sequence was calculated from Eq. (10). Since, the set of parameters correspond to high OQPI indicates the most significant order of input parameters that yields the optimum machining conditions. Hence, the input parameter combination corresponding to the highest grey OQPI was the given the 1st rank and so on. Table 5.4 shows the grey relation coefficient and corresponding OQPI values for each response.

Table 5.8 Grey relational coefficients and OQPI values of output characteristics

Run no.	MRR (mm³/min)	cylindricity error (mm)	Taper (degree)	Surface roughness (µm)	OQPI	Rank
	Grey relational coefficients					
1	0.341751	0.921453	0.368551	0.374435	0.503195	10
2	0.004544	0.940417	0.625132	0.423341	0.437004	17
3	0.636628	0.734831	0.555559	0.305738	0.587744	3
4	0.319368	0.867759	0.688249	0.296278	0.491394	13
5	0.62056	0.56115	0.970734	0.570813	0.577899	5
6	0.018518	0.888141	0.608327	0	0.424901	18
7	0.014883	0.962478	0.781363	0.541998	0.450526	16
8	0.339232	0.958459	0.746286	0.286528	0.520526	7
9	0	0.61295	0.8727	0.09831	0.390064	19
10	0.621724	0.629401	0.943263	0.512667	0.583019	4
11	0.336184	0.904892	0.426398	0.385203	0.498662	11
12	0.677558	0.611397	0.492388	0.403232	0.594729	2
13	0.035226	0.071342	1	1	0.378006	20
14	0.308569	1	0.685596	0.709089	0.525212	6
15	0.339201	0.77436	0.385609	0.558181	0.475292	15
16	1	0	0	0.429122	0.858736	1
17	0.328163	0.983351	0.213715	0.311272	0.513708	8
18	0.41048	0.814246	0.554591	0.344355	0.505877	9
19	0.310231	0.911169	0.567573	0.436567	0.495868	12
20	0.36977	0.809915	0.526512	0.165881	0.490793	14

Therefore, with PCA based grey relational method the complicated multi objective performance characteristics are converted to single performance index called OQPI easily without much computational work and loss of data.
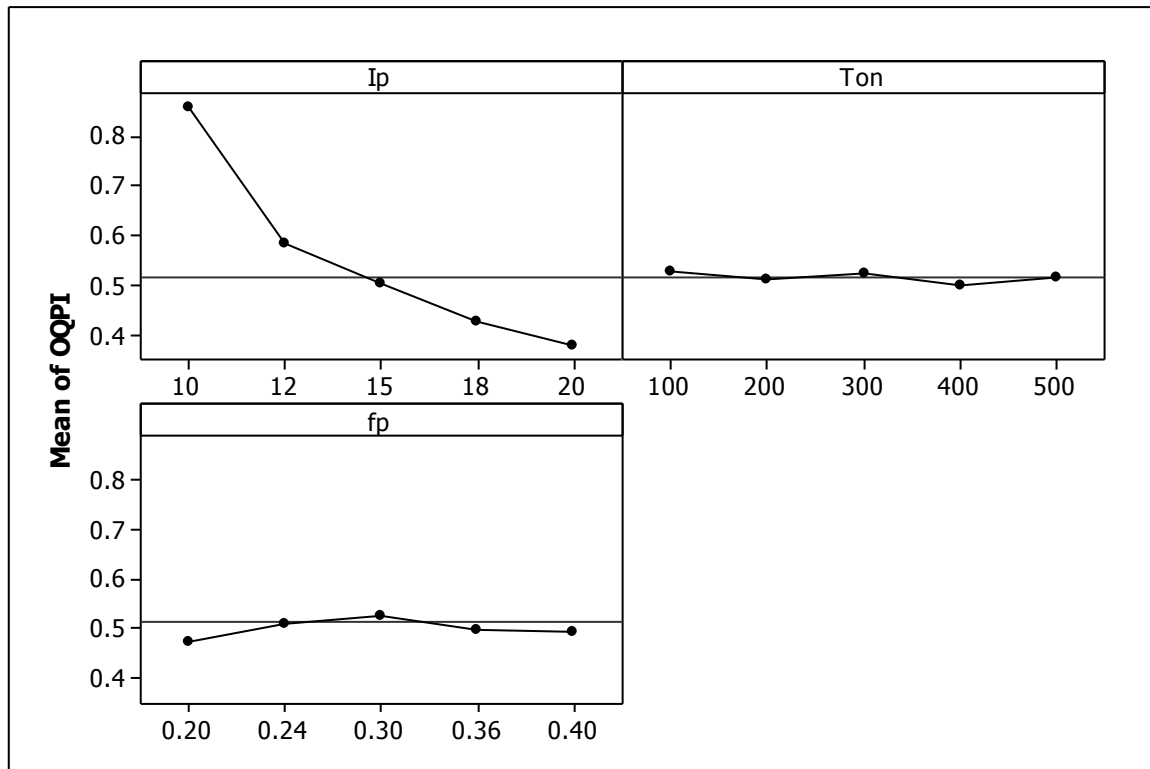
Fig.5.9 Main effect plot for OQPI

Fig. 5.9 represents main effect plot for OQPI with respect to process parameters. From the main effect plots it was found that the optimum machining parameters as $I_p = 10$ A, $T_{on} = 100$ μs and $F_p = 0.3$ kg/cm^2 based on higher OQPI values. Table 5.5 shows the difference of maximum and minimum values of each process parameters i.e. I_p, T_{on} and F_p. Since this difference is highest for peak current, it can be concluded that peak current has significant influence on output responses followed by flushing pressure and pulse-on time.

Table 5.9 Response table for OQPI

Level	process parameters		
	Peak current(I_p) (A)	Pulse-on time (T_{on}) (µs)	Flushing pressure(F_p) (Kg/cm^2)
1	0.85874	0.52521	0.47529
2	0.58558	0.51211	0.51202
3	0.502053	0.52184	0.52864
4	0.425624	0.49936	0.49946
5	0.37800	0.51370	0.49586
max-min	0.48074	0.02585	0.05335
Rank	1	3	2

5.3 Confirmatory tests

Now, the obtained optimum values are tested by confirmatory experiments. It was observed from confirmation test that the optimum parametric combination would result in decrease SR, taper and cylindricity and also observed decrease in MRR as compared to initial parameter setting (Table 5.6). This is because as the main aim of R-EDM is to fabricate arrayed structures with minimum tolerance and high surface quality rather than high MRR. The predicted OQPI value at optimal level can be calculated by Eq. (15).

$$\hat{\delta} = \delta_m + \sum_{i=1}^{r}\left(\delta_i - \delta_m\right) \qquad (15)$$

Where δ_m is mean of OQPI values of all experimental runs, δ_i is the average of OQPI at optimum level of ith parameter and r indicates number of input parameters that are effecting the OQPI.

Table 5.10 Confirmatory test results

Responses	Initial parameter setting levels	Parameter setting levels with higher OQPI	Optimum parameter setting levels	
	$I_p = 12$ A $T_{on} = 400$ μs $F_p = 0.24$ kg/cm^2	$I_p = 10$ A $T_{on} = 300$ μs $F_p = 0.3$ kg/cm^2	$I_p = 10$ A $T_{on} = 100$ μs $F_p = 0.3$ kg/cm^2	
			Predicted	Experimental
MRR (mm^3/min)	34.98	24.76		23.354
SR (μm)	7.2	6.8		5.78
Taper (degree)	10.17	9.24		8.22
Cylindricity error (mm)	0.232	0.1287		0.1154
OQPI	0.5947	0.8587	0.8864	0.8736
Improvement in OQPI			0.2917	0.2789

CHAPTER 6

CONCLUSIONS

In the present study, R-EDM was successfully used in macro domain for fabricating textured surfaces of diameter 3 mm and depth 2 mm on mild steel plates using copper as tool electrode. Effect of different process on response characteristics was investigated using RSM. Grey relational analysis (GRA) in conjunction with principal component analysis (PCA) was used to find the optimal machining conditions. The following conclusions can be summarized from the investigation:

1. Results indicate that MRR was mainly influenced by peak current and pulse-on time during R-EDM of arrayed structures. Peak current being the most significant factor with percentage contribution of 93.49%.

2. Peak current (I_p) has significant effect on the SR, Taper, cylindricity error.

3. Moderate pulse-on time and flushing pressure results in less tapering and cylindricity error.

4. Cross section of the work piece revealed the presence of three zones i.e., recast layer, heat affected zone and base material. Micro hardness close to recast layer is found to be less and it increases with depth and reaches maximum in HAZ and surface morphology of pillared structure has been studied.

5. The optimization results confirmed that peak current has highest influence on output responses followed by flushing pressure and pulse-on time during the R-EDM process.

6. PCA merged GRA showed to be effective in determining the optimal machining conditions in R-EDM involving multi-response characteristics. The recommended level of process parameters for maximization of MRR, minimization of SR , taper as well cylindricity

error during R-EDM of arrayed structures has been found to be $I_p = 10$ A, $T_{on} = 100$ µs and $F_p = 0.3$ kg/cm^2 using PCA based GRA technique.

6.1 Scope of future work

Electrical discharge machining has great potential in fabrication of textured surface of different types and geometry. Following issues may be taken up to further explore the concept

1. Further study is required in order to minimize the dimensional accuracy of textured surface. Online monitoring of R-EDM can be helpful in this area. Effect of reverse tolerance and insulation can be taken for further investigation.

2. Surface integrity of textured surface should be investigated in detail.

3. Exploratory study has been made in case of mild steel but further study can also be carried on advanced materials depending on the specific application.

REFERENCES

[1] Evans, C.J and Bryan, J.B., Structured, Textured or engineered surfaces. CIRP Ann. Manufacturing Technology 1999, 48, 541-555.

[2] Coblas, D. G., Fatu, A., Maoui, A and Hajjam, M., Manufacturing Textured surfaces: State of Art and Recent Developments. Proceedings of the Institution of Mechanical Engineers, Part J: Journal of Engineering Tribology 2014.

[3] Ruprecht, R., Benzler, T., Hanemann, T., Various replication techniques for manufacturing three dimensional metal microstructures, Microsyst Technol 1997, 4, 28–31.

[4] Jeon, N.L., Nuzzo, R.G., Xia. Y., Patterned self- assembled monolayers formed by microcontact printing direct selective metallization by chemical vapor deposition on planar and nonplanar substrates. Langmuir 1995, 21, 3024–3026.

[5] Dowling, A. J., Novel strategies for surface micromachining TiN thin films. PhD Thesis, Swinburne University of Technology, Australia, 2005.

[6] Park, J., Moon, J., Shin, H., Direct-write fabrication of colloidal photonic crystal microarrays by ink-jet printing. J Colloid Interface Sci 2006, 298, 713–719.

[7] Chiffre, L., Kunzmann, H., Peggs, G.N., Surfaces in precision engineering, micro engineering and nano- technology. CIRP Ann. Manufacturing Technology 2003, 52, 561–577.

[8] Liu, H., Wan, D and Hu, D., Microstructure and wear behaviour of laser-textured and micro-alloyed Co-based WC and TiC composite sintered-carbide coating. J Mater Process Technology 2009, 209, 805–810.

[9] Ningsong, Q., Xiaolei, C., Hansong, L., Electrochemical micromachining of micro-dimple arrays on cylindrical inner surfaces using a dry-film photoresist. Chinese J Aeronaut 2014; http:// dx.doi.org/10.1016/j.cja.2014.03.012.

[10] Dewangan, S.K., Experimental investigation of machining parameters for EDM using U-shaped electrode of AISI P20 tool steel, PHD Thesis, NIT Rourkela, 2010.

[11] Pandey, A., and Singh, S., Current research trends in variants of Electrical Discharge Machining: A review. International Journal of Engineering Science 2010, 2(6), 2172–2191.

[12] Crookall, J.R., Heuvelman, C.J., Electro-discharge machining-the state of the art", Annual of the CIRP, 1971, 20, pp.113-120.

[13] Lauwers, B., Kruth, J.P., Liu. W., Investigation of material removal mechanisms in EDM of composite ceramic materials. J Mater Process Technology 2004, 149,347–352.

[14] Godwin, M.J., Application of New Type of EDT for Surface Preparation of Cold Mill Work Rolls; Proc. Advances in Cold Rolling Technology, Institute of Metals, London ,1985, 102-107.

[15] Koshy, P., and J, Tovey., Performance of Electrical Discharge Textured Cutting Tools. CIRP Annals - Manufacturing Technology, 2011, 60(1), 153–56.

[16] Singh. S.K., Chourasia, A., Agarwal, P., Reverse EDM of collective electrodes in micro ECM, 2014, vol. 3, no. 10, pp. 342-346.

[17] Goto, A., Yuzawa, T., Magara, T., and Kobayashi, K., Study on deterioration of machining performance by EDMed sludge and its prevention, International Journal of Machining, 1998, 3 1–6.

[18] Chamaran. F, Yeh. Y, Min. H. S, Dunn. B. Kim. C. J, Fabrication of high - aspect – ratio electrode arrays for the three-dimensional micro batteries, Journal of Micromechanical systems, 2007, 844-853.

[19] Joshi, S. S., Mujumdar, S., Mastud, S., Singh, R. K., Experimental characterization of reverse micro- electric discharge machining process for machining of aspect ratio micro rod arrays, IMech Journal of Engineering Manufacture: Part-B,2009,778- 794.

[20] Wang, Z., Cao, G., Zhang, Y., Zhao, W., Research on reversible electric discharge removal and deposition machining in gas, Jixie Gongcheng Xuebao/Chinese J. Mech. Eng., vol. 40, 2004, pp. 88–92.

[21] Kim, B., Park, B., Chu. C., Fabrication of multiple electrodes by reverse EDM and their application in micro – ECM, Journal of Micromechanics and Micro engineering, 2006, 843-850.

[22] Yi, S., Park, M., Lee, Y., Chu, C., Fabrication of a stainless steel shadow mask using batch mode micro – EDM, Microsystems Technology, 2008, 411 – 417.

[23] Zeng, W. L., Gong, Y. P., Liu, Y., Wang, Z. L., Experimental study of micro electro array and micro-hole array fabrication by ultrasonic enhanced micro – EDM, Key Engineering Materials, 2008, 482 – 487.

[24] Hwang, Y. L., Kuo, C. L., Hwang, S. F., Fabrication of a micro pin array with high density and high hardness by combining mechanical peck – drilling and reverse EDM, J.Mater. Process. Technology, 2010, 24 – 27.

[25] Mastud, S., Singh, R. K., Joshi, S. S, Analysis of fabrication of arrayed micro rods on WC using reverse micro – EDM, In Proceedings of the International Workshop on Micro factories (IWMF), 2010, 24- 27.

[26] Jin, B. D., Cao, G., Wang, Z. L., Zhao. W. S., A micro deposition method by using EDM, Key Eng. Mater, 2007, 32 – 36.

[27] Fofonoff, T. A., Martel, S. M., Hatsopoulos, N. G., Donoghue, J. P., Hunter, I. W., Micro electrode array fabrication by electrical discharge machining and chemical etching, IEEE Trans. Biomed. Eng, 2004, 890 – 895.

[28] Takahata, K., Gianchandani, Y. B., Batch mode micro electro discharge machining, J. Micro ElectroMech. Syst (2002) 102 – 110.

[29] Singh. R, Characterization of Micro- EDM process for Pyrolytic Carbon, Proceedings of the world congress on Engineering, 2008.

[30] Mastud, S. A., Kothari, S. N., Singh, R. K., Samuel, J., Joshi, S. S., Analysis of debris motion in vibration assisted reverse micro electrical discharge machining, Materials, Micro and Nano Technologies, Properties, Applications and Systems; Sustainable Manufacturing, 2014, Vol. 1, p.V001T3A017.

[31] Weiliang, Zeng., Zhenlong, Wang., Experimental Study of Microelectrode Array and Micro-hole Array Fabricated by Ultrasonic Enhanced Micro-EDM. Key Engineering Materials, 2008, 364-366, 482.

[32] Singh, S. K., Chourasia, A., Agarwal, P., Reverse EDM of collective electrodes and their applications in micro ECM,2014, 342 – 346.

[33] Peng, Z., Wang, Z., Dong, Y. & Chen, H. Development of a reversible machining method for fabrication of microstructures by using micro-EDM. J. Mater. Process. Technol. 2010, 129-136.

[34] Zilong, P.L., Wang, Z.L., Jin, B.D., Micro-forming process and microstructure of deposit by using micro EDM deposition in air. Key Eng. Mater, 2008, 153–157.

[35] Liao, Y. S., Chang, T. Y., and Chuang, T. J. An on-line monitoring system for a micro electrical discharge machining (micro-EDM) process. J. Micromech. Microeng. 2008, 18, 1-9.

[36] Mastud, S. A., Garg, M., Singh, R. & Joshi, S. S. Recent developments in the reverse micro-electrical discharge machining in the fabrication of arrayed micro-features. Proc. Inst. Mech. Eng. Part C J. Mech. Eng. Sci.,2011**,** 367–384.

[37] Bhattacharyya, B, Gangopadhyay. S, Sarkar. B R, Modelling and analysis of EDMed job surface integrity, Journal of Materials Processing Technology, 2007, 169-177.

[38] Gowda. B. M, Ravindra. H. V, Jain. S. P, Raj. M. N, Comparative study of surface roughess and cylindricity of aluminium silicon nitride material using MRA GMDH and pattern recognition technique in drilling, Procedia Mater. Sci, 2014, 1770 – 1779.

[39] Dewngan. S, Biwas. C.K., Gangopadhyay. S, Optimization of EDM process parameters using PCA based Grey Relation Investigation, Procidia Mater. Sci, 2014, 1091 – 1096.

[40] Singh. A, Anandita. S, Gangopadhyay S, Microstructural analysis and Multi Response Optimization during ECM of Inconel 825 using hybrid approach, Material and Manufacturing Processes, 2014, 37 – 41.